Eidgenössische Technische Hochschule Zürich

Ecole polytechnique fédérale de Zurich
Politecnico federale di Zurigo
Swiss Federal Institute of Technology Zurich

Boundary Conditions for Regularized 13-Moment-Equations for Micro-Channel-Flows

Manuel Torrilhon and Henning Struchtrup[†]

Research Report No. 2008-14
May 2008

Seminar für Angewandte Mathematik
Eidgenössische Technische Hochschule
CH-8092 Zürich
Switzerland

[†]Dept. of Mechanical Engineering, University of Victoria, Canada / Institute of Polymer Physics, ETH Zurich, Switzerland/ mail: struchtr@uvic.ca

Boundary Conditions for Regularized 13-Moment-Equations for Micro-Channel-Flows

Manuel Torrilhon and Henning Struchtrup[†]

Seminar für Angewandte Mathematik
Eidgenössische Technische Hochschule
CH-8092 Zürich
Switzerland

Research Report No. 2008-14 May 2008

Abstract

Boundary conditions are the major obstacle in simulations based on advanced continuum models of rarefied and micro-flows of gases. In this paper we present a theory how to combine the regularized 13-moment-equations derived from Boltzmann's equation with boundary conditions obtained from Maxwell's kinetic accommodation model. While for the linear case these kinetic boundary conditions suffice, we need additional conditions in the non-linear case. These are provided by the bulk solutions obtained after properly transforming the equations while keeping their asymptotic accuracy with respect to Boltzmann's equation.

After finding a suitable set of boundary conditions and equations, a numerical method for generic shear flow problems is formulated. Several test simulations demonstrate the stable and oscillation-free performance of the new approach.

[†]Dept. of Mechanical Engineering, University of Victoria, Canada / Institute of Polymer Physics, ETH Zurich, Switzerland/ mail: struchtr@uvic.ca

1 Introduction

Gas flows in rarefied situations or micro-scale settings cannot be described by classical fluid models like the system of Navier-Stokes-Fourier (NSF). This is due to lack of sufficiently many collisions of particles, i.e., the Knudsen number − the ratio of mean free path and macroscopic length − is too large and the flow cannot be considered to be near equilibrium. Instead, the statistical approach of kinetic gas theory is required to model those processes as described, e.g., in the textbooks [7], [8] and [38]. Moment equations as introduced by Grad [10], [11] offer a possibility to reduce the complex statistical description of kinetic theory to a continuum model for macroscopic fields, see [3], [19]. Various modifications have been proposed, e.g., in [9], [13], [16] and [20].

The regularized 13-moment-equations (R13) derived in [31] may be considered as the most promising extension of Grad's equations. They combine high physical accuracy and stability, see [37], [36]. Moreover, R13 was shown to satisfy a consistent ranking in terms of orders of magnitude, see [28], and an entropy inequality in the linear case [32]. Especially due to its stability, the R13-system succeeds over models obtained by high-order Chapman-Enskog expansion as used, e.g., in [2], [17] and [39]. In general, high-order Chapman-Enskog expansions are proven to be linearly unstable [5], [23]. See the textbook [26] for an overview of different model equations in kinetic gas theory.

Due to the modelling successes, the interest in computations based on moment equations is vivid, e.g., in [1], [21], [24] and [33]. Computational methods for the R13-system have been proposed in [35] for the initial value problem and in [12] for the boundary value problem. The major obstacle to overcome in simulations is the modelling of suitable boundary conditions. Here, the paper of Gu and Emerson [12] may be regarded as pioneering work. They showed that moment relations obtained from an accommodation model are in principle sufficient to describe boundary conditions for R13. However, in their work inconsistencies occur and oscillations are reported which are likely due to insufficient modelling of the boundary.

The present paper establishes a theory of boundary conditions for the regularized 13-moment-equations based on physical and mathematical requirements for the system. As general setting we shall consider shear flows in a parallel channel. In spite of the apparent one-dimensional character of the setting, the full two-dimensional set of R13-variables is involved. This makes the process a relevant model also for more complex computations. For boundary conditions, we follow the approach originally given by Grad in [10] based on the kinetic accommodation model of Maxwell [18], similar to the approach in [12]. This gives a certain number of boundary conditions. However, the mathematical structure of the equations shows that the linear and non-linear cases require different numbers of boundary conditions. Our major hypothesis is that, instead of finding additional boundary conditions for the non-linear case, the equations should be transformed such that the number of required boundary conditions remains the same. To be precise, the transformed equations will supply additional conditions which complement the boundary conditions, also in the untransformed case. The transformation of the system is possible as long as we require the asymptotic accuracy of the system in terms of the Knudsen number to stay the same. The asymptotic accuracy is given by the comparison of the Chapman-Enskog-expansion of the R13-system with the Chapman-Enskog-expansion of the Boltzmann equation. We shall use the fact that higher order terms in the R13-equations may be changed

without changing the accuracy. Linear stability is also unaffected by this, since only non-linear terms are changed. This is sufficient to find a stable system suitable for the boundary conditions that are available.

In general, emphasis will be put on the additional inherent conditions for specific variables that are obtained by this method. These relations represent bulk solutions of moments that can not produce a boundary layer due to restriction to a finite set of moments. We include an interpretation of the whole method along these lines.

After finding a suitable combination of boundary conditions and transformed equations, a numerical method is developed based on the R13-system written as a first order system. Incorporation of the boundary conditions is straightforward. An empirical convergence study shows second order numerical accuracy of the method. Various simulation results for channel flows of Couette- and Poiseuille-type demonstrate stable and oscillation-free behavior. Comparison with DSMC simulations of Boltzmann's equation, see [4], show accurate agreement for slow flows and moderate Knudsen numbers.

The rest of the paper is organized as follows: Sec. 2 presents the R13 equations and their specialization to steady shear flow. It also discusses the asymptotic accuracy. Sec. 3 is devoted to the theory of boundary conditions with physical and mathematical remarks, a review of kinetic boundary conditions and the presentation of our major hypotheses. The linear case of the R13-system is studied in detail in Sec. 4. The insights of the linear case are generalized to the non-linear case in two steps in Sec. 5.1 and Sec. 5.2. A deeper interpretation of the formal procedure is given in Sec. 5.4. The numerical method is described in Sec. 6 and results are discussed in Sec. 7. An appendix provides a number of detailed bulky matrices which are left out in the main part for readability.

2 R13 equations

Details of the derivation of the R13 equations for rarefied/micro-flows can be found in [31] and the textbook [26]. Here we only give the final equations.

2.1 Full Equations

The basis of the R13 system is given by the conservation laws of mass, momentum and energy,

$$\begin{aligned} \partial_t \rho + \operatorname{div}(\varrho \mathbf{v}) &= 0, \\ \partial_t \rho\mathbf{v} + \operatorname{div}\left(\rho\mathbf{v}\mathbf{v}^T + p\mathbf{I} + \sigma\right) &= \rho\,\mathbf{f}, \\ \partial_t\left(\rho\varepsilon + \tfrac{1}{2}\rho\mathbf{v}^2\right) + \operatorname{div}\left(\rho\varepsilon\mathbf{v} + \tfrac{1}{2}\rho\mathbf{v}^2\mathbf{v} + p\mathbf{v} + \sigma\mathbf{v} + \mathbf{q}\right) &= \rho\,\mathbf{f}\cdot\mathbf{v} \end{aligned} \tag{1}$$

where we take the internal energy $\rho\varepsilon = \frac{3}{2}p$ for monatomic gases and the temperature θ (in energy units) satisfies the ideal gas law $p = \rho\,\theta$. An external body force density is given by $\rho\mathbf{f}$. The R13 equations can be viewed as a generalized constitutive theory for stress tensor σ and heat flux $\mathbf{q}$. The standard local relations of Navier-Stokes and Fourier are extended to form full evolution equations for σ_{ij} and q_i. They are given by

$$\frac{\partial\sigma_{ij}}{\partial t} + \frac{\partial\sigma_{ij}v_k}{\partial x_k} + \frac{4}{5}\frac{\partial q_{\langle i}}{\partial x_{j\rangle}} + 2p\frac{\partial v_{\langle i}}{\partial x_{j\rangle}} + 2\sigma_{k\langle i}\frac{\partial v_{j\rangle}}{\partial x_k} + \frac{\partial m_{ijk}}{\partial x_k} = -\frac{p}{\mu}\sigma_{ij} \tag{2}$$

for the stress tensor, and

$$\frac{\partial q_i}{\partial t} + \frac{\partial q_i v_k}{\partial x_k} + p\frac{\partial(\sigma_{ik}/\rho)}{\partial x_k} + \frac{5}{2}(p\delta_{ik}+\sigma_{ik})\frac{\partial \theta}{\partial x_k} - \frac{\sigma_{ij}}{\varrho}\frac{\partial \sigma_{jk}}{\partial x_k} + q_k\frac{\partial v_i}{\partial x_k} + (m_{ijk} + \frac{6}{5}q_{(i}\delta_{jk)})\frac{\partial v_j}{\partial x_k} + \frac{1}{2}\frac{\partial \hat{R}_{ik}}{\partial x_k} = -\frac{2p}{3\mu}q_i \quad (3)$$

for the heat flux. Both equations form quasi-linear first order equations with relaxation. The collision frequency is given by p/μ with viscosity μ. Indices with angular brackets indicate the trace-free symmetric parts of a tensor, while round brackets indicate symmetrized tensors [26].

The remaining unspecified quantities are m_{ijk} and $\hat{R}_{ij}$. They stem from higher moments contributions in the transfer equations of Boltzmann's equation. Neglecting these contributions, i.e., setting $m_{ijk} = \hat{R}_{ij} = 0$, turns the system (1)-(3) into the classical 13-moment-case of Grad [10], [11]. In [31] gradient expressions are derived for m_{ijk} and $\hat{R}_{ij}$ which regularize Grad's equations and turn them into a highly accurate micro-flow model. The regularization procedure gives

$$\begin{aligned} m_{ijk} &= -2\mu\,\frac{\partial(\sigma_{\langle ij}/\rho)}{\partial x_{k\rangle}} + \frac{8}{10p}q_{\langle i}\sigma^{(\mathrm{NSF})}_{jk\rangle}\ , \\ R_{ij} &= -\frac{24}{5}\mu\,\frac{\partial(q_{\langle j}/\rho)}{\partial x_{j\rangle}} + \frac{32}{25p}q_{\langle i}q^{(\mathrm{NSF})}_{j\rangle} + \frac{24}{7\rho}\sigma_{k\langle i}\sigma^{(\mathrm{NSF})}_{j\rangle k}\ , \\ R &= -12\mu\,\frac{\partial(q_k/\rho)}{\partial x_k} + \frac{8}{p}q_k q^{(\mathrm{NSF})}_k + \frac{6}{\rho}\sigma_{ij}\sigma^{(\mathrm{NSF})}_{ij}\ . \end{aligned} \quad (4)$$

with $\hat{R}_{ij} = R_{ij} + \frac{1}{3}R\delta_{ij}$ and the abbreviations

$$\sigma^{(\mathrm{NSF})}_{ij} = -2\mu\,\frac{\partial v_{\langle i}}{\partial x_{j\rangle}}, \qquad q^{(\mathrm{NSF})}_i = -\frac{15}{4}\mu\,\frac{\partial \theta}{\partial x_i}. \quad (5)$$

Note the special structure in (4): The leading expressions are gradient terms that produce Laplacians of stress and heat flux in their respective equations in (2)/(3). This is similar to the Navier-Stokes-Fourier system which can be viewed as regularization of the Euler equations. The next terms in (4) are products of the stress and heat flux with velocity and temperature gradients. In (4) we left out higher order contributions following [28].

Equations (1)-(4) with (5) form the system of regularized 13-moment-equations.

2.2 Relation to Boltzmann's equation and Navier-Stokes-Fourier

We will briefly discuss how the R13 system is related to the equations of Navier-Stokes-Fourier, and Boltzmann's equation. These results were obtained in [31] and [37] based on asymptotic analysis.

The mean collision frequency $\nu = \frac{p}{\mu}$ appears on the right hand side of the equations (2), (3). Introducing the mean free path at a reference state by

$$\lambda_R = \frac{\mu_R\sqrt{\theta_R}}{p_R} \quad (6)$$

we define the Knudsen number

$$Kn = \frac{\lambda_R}{L} = \frac{\mu_R\sqrt{\theta_R}}{p_R L} \tag{7}$$

based on a macroscopic length scale L. The isothermal equilibrium speed of sound $\sqrt{\theta_R}$ gives a natural velocity scale for the equations and all moment variables can be scaled by a reference density ρ_R and appropriate powers of $\sqrt{\theta_R}$. By defining a time scale by $T = L/\sqrt{\theta_R}$ we can write the equations in dimensionless form and the Knudsen number only appears as factor 1/Kn at the right hand side.

Based on the Knudsen number we can derive an *asymptotic accuracy* of the R13 system with respect to Boltzmann's equation. This is done by expanding stress tensor and heat flux in powers of $Kn < 1$ for both R13 and Boltzmann. In the case of Maxwell molecules we find

$$\left\|\sigma^{(\mathrm{R13})} - \sigma^{(\mathrm{Boltz})}\right\| + \left\|\mathbf{q}^{(\mathrm{R13})} - \mathbf{q}^{(\mathrm{Boltz})}\right\| = \mathcal{O}\left(Kn^4\right) \tag{8}$$

with any appropriate norms for stress and heat flux. This means that any R13 result will differ asymptotically from a full Boltzmann simulation only in $\mathcal{O}\left(Kn^4\right)$ in the Chapman-Enskog sense. In the language of [28] this corresponds to third order equations. For comparison we note that for the laws of Navier-Stokes and Fourier (5) we obtain only

$$\left\|\sigma^{(\mathrm{NSF})} - \sigma^{(\mathrm{Boltz})}\right\| + \left\|\mathbf{q}^{(\mathrm{NSF})} - \mathbf{q}^{(\mathrm{Boltz})}\right\| = \mathcal{O}\left(Kn^2\right). \tag{9}$$

This also shows that NSF is asymptotically included in R13 for small Knudsen numbers, i.e., for very small Knudsen numbers the R13 system will essentially behave like the NSF equations.

The viscosity μ in (2), (3) links the R13 system to NSF in the asymptotic limit. For power law potentials the viscosity is given by

$$\mu = \mu_R \left(\frac{\theta}{\theta_R}\right)^{\omega} \tag{10}$$

with a temperature exponent $0.5 \leq \omega \leq 1$.

2.3 Equations for Steady Shear Flow

This paper considers processes that fall into the class of steady shear flows, including steady Couette or Poiseuille flows. For the R13 system, shear flow is a multi-dimensional phenomenon in the sense that it produces a fully multi-dimensional reaction for the stress tensor and heat flux. Introducing $x_i \hat{=} (x, y, z)$, we consider shear flow which is homogeneous in z-direction and define the remaining non-vanishing parts of stress tensor and heat flux as

$$\sigma = \begin{pmatrix} \sigma_{xx} & \sigma & 0 \\ \sigma & \sigma_{yy} & 0 \\ 0 & 0 & \sigma_{zz} \end{pmatrix}, \quad \mathbf{q} = (q_x, q_y, 0) \tag{11}$$

where $\sigma = \sigma_{xy} = \sigma_{yx}$, and $\sigma_{zz} = -\frac{1}{2}(\sigma_{xx} + \sigma_{yy})$ since σ must be trace-free. For the velocity we assume $v_y = v_z = 0$ and

$$\mathbf{v}\,(x, y, z) = (v_x\,(y)\,, 0, 0)\,. \tag{12}$$

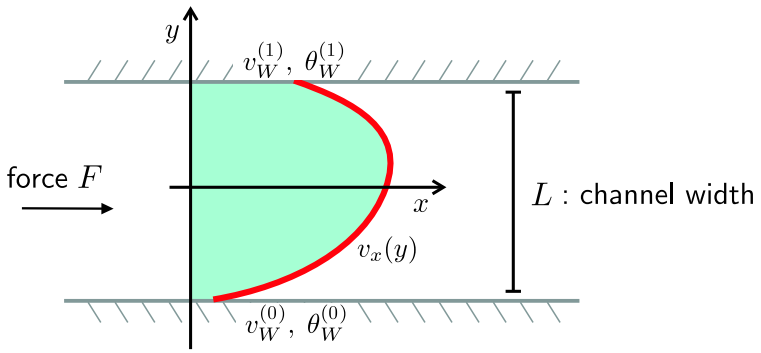

Figure 1: General shear flow setting. The gas flows between infinte plates with velocities $v_W^{(0,1)}$ and temperature $\theta_W^{(0,1)}$. The force F is given by gravity or a pressure gradient.

The force acts only in x-direction, $\mathbf{f} = (F, 0, 0)$. This setting is valid for channel flows as displayed in Fig. 1. The gas is confined between two infinite plates at distance L and is moving solely in x-direction. As driving force either a force F in x-direction is given or the walls are moving with x-velocities $v_W^{(0,1)}$. In the simplest case the force can be viewed as gravity but it may also stem from a homogeneous pressure gradient along the x-axis. Additionally, the walls may be kept at different temperatures $\theta_W^{(0,1)}$.

In this setting we have 8 independent variables in the R13 equations, namely $\{\rho, v_x, p, \sigma_{xx}, \sigma_{yy}, \sigma, q_x, q_y\}$. Optionally, the pressure p can be replaced by the temperature θ. The 5 remaining relevant constitutive quantities are $\left\{m_{xxy}, m_{xyy}, m_{yyy}, \hat{R}_{xy}, \hat{R}_{yy}\right\}$. The system (1)-(4) reduces to 13 first order non-linear ordinary differential equations.

The core equations are given by the conservation laws

$$\partial_y \sigma = \rho F\,, \tag{13}$$
$$\partial_y (p + \sigma_{yy}) = 0\,, \tag{14}$$
$$\partial_y q_y + \sigma\, \partial_y v_x = 0\,, \tag{15}$$

the balance of stress tensor

$$2\sigma\, \partial_y v_x + \frac{2}{5}\partial_y q_y + \partial_y m_{xxy} = -\frac{p}{\mu}\sigma_{xx}\,, \tag{16}$$
$$\frac{6}{5}\partial_y q_y + \partial_y m_{yyy} = -\frac{p}{\mu}\sigma_{yy}\,, \tag{17}$$
$$(p + \sigma_{yy})\partial_y v_x + \frac{2}{5}\partial_y q_x + \partial_y m_{xyy} = -\frac{p}{\mu}\sigma\,, \tag{18}$$

and heat flux balance

$$\frac{p-\sigma_{xx}}{\rho}\partial_y\sigma+\frac{5}{2}\sigma\partial_y\theta-\frac{\sigma}{\rho}\partial_y\sigma_{yy}-\frac{\sigma}{\rho}\theta\partial_y\rho+(m_{xxy}+\frac{7}{5}q_y)\partial_y v_x+\frac{1}{2}\partial_y\hat{R}_{xy}=-\frac{2p}{3\mu}q_x\,, \tag{19}$$

$$\frac{p-\sigma_{yy}}{\rho}\partial_y\sigma_{yy}+\frac{5}{2}(p+\sigma_{yy})\partial_y\theta-\frac{\sigma}{\rho}\partial_y\sigma-\frac{\sigma_{yy}}{\rho}\theta\partial_y\rho+(m_{xyy}+\frac{2}{5}q_x)\partial_y v_x+\frac{1}{2}\partial_y\hat{R}_{yy}=-\frac{2p}{3\mu}q_y\,. \tag{20}$$

For the constitutive equations we note that (5) has non-vanishing contributions only for $\sigma^{(\mathrm{NSF})}=-\mu\,\partial_y v_x$, and $q_y^{(\mathrm{NSF})}=-\frac{15}{4}\mu\,\partial_y\theta$. With this we find from (4) five equations for m_{ijk} and $\hat{R}_{ij}$,

$$-\frac{p}{\mu}m_{xxy}=\frac{2}{3}p\,\partial_y(\sigma_{xx}/\rho)-\frac{4}{15}p\,\partial_y(\sigma_{yy}/\rho)+\frac{32}{75}q_x\partial_y v_x\,, \tag{21}$$

$$-\frac{p}{\mu}m_{yyy}=\frac{6}{5}p\,\partial_y(\sigma_{yy}/\rho)-\frac{8}{25}q_x\partial_y v_x\,, \tag{22}$$

$$-\frac{p}{\mu}m_{xyy}=\frac{16}{15}p\,\partial_y(\sigma/\rho)+\frac{32}{75}q_y\partial_y v_x\,, \tag{23}$$

and

$$-\frac{p}{\mu}\hat{R}_{xy}=\frac{12}{5}p\,\partial_y(q_x/\rho)+\frac{12}{5}q_x\partial_y\theta+\frac{12}{7}\theta(\sigma_{xx}+\sigma_{yy})\partial_y v_x\,, \tag{24}$$

$$-\frac{p}{\mu}\hat{R}_{yy}=\frac{36}{5}p\,\partial_y(q_y/\rho)+\frac{66}{5}q_y\partial_y\theta+\frac{36}{7}\theta\,\sigma\,\partial_y v_x\,. \tag{25}$$

The system (13)-(25) has to be complemented by boundary conditions.

3 Theory of Boundary Conditions

3.1 Mathematical Remarks

The above system (13)-(25) can be written in matrix form as

$$\mathbf{A}\,(\mathbf{U})\;\partial_y\mathbf{U}=\mathbf{P}\,(\mathbf{U}) \tag{26}$$

where $\mathbf{U}=\{\rho,v_x,p,\sigma_{xx},\sigma_{yy},\sigma,q_x,q_y,m_{xxy},m_{yyy},m_{xyy},R_{xy},R_{yy}\}$. The full system is displayed in (91) in the Appendix. The matrix $\mathbf{A}$ is rather bulky but it provides a good overview about the coupling in the equations.

Consider the formal *initial* value problem for (26), i.e., the one-sided boundary value problem where we only prescribe values at $y=0$. If N is the dimension of the system and the matrix $\mathbf{A}(\mathbf{U})$ has an eigenvalue $\lambda=0$ with multiplicity α, then we can describe $N-\alpha$ initial conditions for $\mathbf{U}$. Indeed, the zero eigenvalue induces left eigenvectors $\{\mathbf{x}_i\}_{i=1,...\alpha}$ with $\mathbf{x}_i\cdot\mathbf{A}(\mathbf{U})=0$, hence, if applied to the system (26), conditions of the form $\mathbf{x}_i\cdot\mathbf{P}(\mathbf{U})=0$ for $i=1,...\alpha$. These conditions can be viewed as constraints for $\mathbf{U}$, which reduce the number of possible initial conditions to $N-\alpha$. In practice, these conditions can be used to eliminate α components of the variable

vector $\mathbf{U}$ and transform (26) into a system of smaller dimension with non-singular matrix. This strategy will be exploited in the next sections for the R13 equations.

The case of a boundary value problem is threatened by non-existence and non-uniqueness. However, in the linear case the argument of the initial value problem carries over and one may prescribe $N-\alpha$ boundary conditions altogether, i.e., if there are n conditions on the left side, only $N-\alpha-n$ conditions on the right side are allowed. In the non-linear case, we are confident that the physical nature of the problem provides us with existence and uniqueness, but rigorous statements for the full system are hard to obtain.

3.2 Kinetic Boundary Conditions

In kinetic theory the fundamental quantity is the velocity distribution function $f(\mathbf{c}, \mathbf{x}, t)$ which is governed by Boltzmann's equation. Wall boundaries require that the incoming half of the distribution function (with $\mathbf{n}\cdot\mathbf{c} > 0$, $\mathbf{n}$ wall normal pointing into the gas) have to be prescribed.

The most common boundary condition for f is Maxwell's accommodation model [18]. It assumes that a fraction χ of the particles that hit the wall are accommodated at the wall and injected into the gas according to a distribution function of the wall f_W. This distribution function is further assumed to be Maxwellian

$$f_W(\mathbf{c}) = \frac{\rho_W/m}{\sqrt{2\pi\theta_W}^3} \exp\left(-\frac{(\mathbf{c}-\mathbf{v}_W)^2}{2\theta_W}\right) \tag{27}$$

with θ_W and $\mathbf{v}_W$ given by the known temperature and velocity of the wall. The "wall density" ρ_W follows from particle conservation at the wall. The remaining fraction $(1-\chi)$ of the particles are specularily reflected. Since the particles that hit the wall are described by a distribution function f_{gas} the reflected part will satisfy a analogous distribution function $f_{\text{gas}}^{(*)}$ which follows from f_{gas} with accordingly transformed velocities.

From this model the velocity distribution function $\tilde{f}(\mathbf{c})$ in the infinitesimal neighborhood of the wall is given by

$$\tilde{f}(\mathbf{c}) = \begin{cases} \chi\, f_W(\mathbf{c}) + (1-\chi)\, f_{\text{gas}}^{(*)}(\mathbf{c}) & \mathbf{n}\cdot(\mathbf{c}-\mathbf{v}_W) > 0 \\ f_{\text{gas}}(\mathbf{c}) & \mathbf{n}\cdot(\mathbf{c}-\mathbf{v}_W) < 0 \end{cases} \tag{28}$$

where $\mathbf{n}$ is the wall normal pointing into the gas. This boundary conditions is used in the majority of simulations based on Boltzmann equation or DSMC [4]. The accommodation coefficient χ describes the wall characteristics and has to be given or measured. The case of $\chi = 0$ (specular reflection) represents the generalization of an adiabatic wall (no heat flux, no shear stress) to the kinetic picture.

3.3 Physical Remarks

The boundary in shear flow problems is governed by two well known effects, velocity slip and temperature jump, and the Knudsen layer, see, e.g., the text books [7] or [26]. Both phenomena become relevant only for rarefied or micro-flows, see [14].

Fig. 2 shows a generic sketch of the situation at the wall. The temperature and velocity jump leads to the fact that the values for θ_W and v_W in the wall will not be assumed in the gas due to

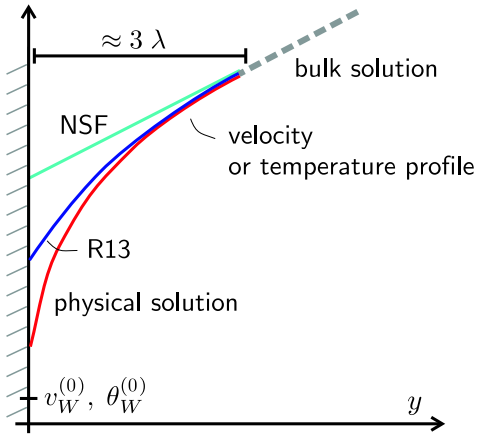

Figure2: Example of velocity or temperature jump and Knudsen layer near the boundary. Only a few mean free pathes away from the wall a near equilibrium solution (bulk solution) is obtained. Velocity and temperature jumps have to be corrected for macroscopic models like NSF or R13.

lack of collisions. These jumps can not be deduced from the transport equations alone, but need to be introduced by the model of the boundary conditions. The Knudsen layer links the strong non-equilibrium at the wall to the bulk solution away from the boundary. The non-equilibrium at the wall can be deduced from the boundary condition for the distribution function (28). Directly at the wall the distribution function is discontinuous in velocity space and as such far from a Maxwellian representing equilibrium. Only after sufficiently many collisions, away from the wall a distribution function close to a Maxwellian will be present. The solution in some distance from the wall is called bulk solution [34].

Different fluid models will describe the Knudsen layer with different accuracy. The equations of Navier-Stokes-Fourier cannot describe a Knudsen layer at all. In this case, the jump conditions are adjusted such that the solution fits to the bulk solution [25], see Fig. 2. The R13 equations allow for some part of the Knudsen layer but misses out higher order modes [27]. Hence, any jump conditions for R13 have to be modified in a way similar to that of NSF.

3.4 Grad's Theory

Any equations for moments are derived from kinetic gas theory. The fundamental assumption is that the kinetic model (28) will also supply meaningful boundary conditions for moment equations.

3.4.1 Accommodation Model

When deriving moment equations Grad also discussed boundary conditions, see [10], [11]. The idea is to take the accommodation model (28) seriously and compute boundary conditions for moments from it.

Indeed, integration of the wall distribution function (28) after multiplication with any velocity

function $\psi(\mathbf{C})$ results in an equation relating moments at the wall to the wall properties given by f_W. We define $\Omega = \{\mathbf{C} \in \mathbb{R}^3\}$ and $\Omega^{\pm} = \{\mathbf{C} \in \mathbb{R}^3 \mid \mathbf{C}\cdot\mathbf{n} \gtrless 0\}$ with wall normal $\mathbf{n}$ as integration domains and find after some rearrangement

$$\int_{\Omega} \psi(\mathbf{C})\, \tilde{f}(\mathbf{C})\, d\mathbf{C} = \int_{\Omega^-} \left(\psi(\mathbf{C}) + (1-\chi)\,\psi_*(\mathbf{C})\right) f_{\text{gas}}(\mathbf{C})\, d\mathbf{C} + \chi \int_{\Omega^+} \psi(\mathbf{C}_W - \mathbf{V})\, f_W(\mathbf{C}_W)\, d\mathbf{C}_W. \tag{29}$$

The first two integrals are evaluated in the frame moving with the gas average velocity $\mathbf{v}_{\text{gas}}$ and the particle velocity $\mathbf{c}$ is transformed into the peculiar velocity $\mathbf{C} = \mathbf{c} - \mathbf{v}_{\text{gas}}$. The last integral is evaluated in the frame moving with the velocity of the wall $\mathbf{v}_W$ and the peculiar velocity is given by $\mathbf{C}_W = \mathbf{c} - \mathbf{v}_W$. Due to these transformations the slip velocity $\mathbf{V} = \mathbf{v}_{\text{gas}} - \mathbf{v}_W$ appears which satisfies $\mathbf{n}\cdot\mathbf{V} = 0$. The function ψ_* is defined by

$$\psi_*(\mathbf{C}) = \psi(\mathbf{C} - 2(\mathbf{n}\cdot\mathbf{C})\mathbf{n}) \tag{30}$$

and represents the evaluation of ψ for the specularily reflected values of $\mathbf{C}$.

The relation (29) can now be evaluated by assuming a specific model for the distribution function, e.g., the regularized 13 moment distribution function f_{R13}. We set $\tilde{f} = f_{\text{gas}} = f_{\text{R13}}$ and different polynomials for ψ give boundary conditions for moments. This strategy is proposed in [26] and used in [12]. We will further specify and evaluate the strategy in the following.

3.4.2 Shear Flow Boundary Conditions

Before we continue, we specify the wall normal $\mathbf{n} = (0,1,0)$ and the wall velocity $\mathbf{v}_W = (v_W, 0, 0)$. This corresponds to the lower wall in Fig. 1. With these specifications we also have $\psi_*(\mathbf{C}) = \psi(C_x, -C_y, C_z)$. The generalization to arbitrary walls is straightforward.

The problem with (29) is that it describes too many boundary conditions if we count it on both walls for all functions ψ that produce a variable of the theory. Indeed, if we fix $\tilde{f} = f_{\text{gas}} = f_{\text{R13}}$, every polynomial for ψ would give us a new relation for our moments on the boundary. The first step is to restrict ourselves to those ψ that represent fluxes in our equations. This is motivated from the theory of balance laws which states that at the boundary fluxes, not variables, need to be prescribed. The C-polynomials that occur as y-fluxes in the two-dimensional R13 equations are $\{C_y,\, C_xC_y,\, C_y^2,\, C^2C_y,\, C_x^2C_y,\, C_y^3,\, C_xC_y^2,\, C^2C_xC_y,\, C^2C_y^2\}$. To restrict this list further, we follow an important observation of Grad [10]: If there is no accommodation at all, $\chi = 0$, any polynomial of even degree in C_y will produce an identity in (29). Hence, moments of even degree cannot be controlled when $\chi = 0$. In order to have continuity of the boundary conditions for $\chi \to 0$, we must formulate boundary conditions only for ψ's that are of odd degree in C_y.

This leaves us with 6 candidates for ψ which we rearrange and linearly recombine to give

$$\psi(\mathbf{C}) \in \left\{ C_y, C_xC_y, \left(C^2 - 7\theta\right) C_xC_y, C^2C_y, \left(C_y^2 - \frac{3}{5}C^2\right) C_y, \left(C_x^2 - C_z^2 - \frac{2}{5}C^2\right) C_y \right\}. \tag{31}$$

These polynomials represent the fluxes $\{v_y, \sigma, R_{xy}, q_y, m_{yyy}, m_{xxy} - m_{yzz}\}$. The first one, v_y, gives the conservation of mass at the wall and, thus, a relation for the value of ρ_W in (27). For the distribution function of the R13 equations, see Appendix C, we find

$$P := \sqrt{\theta}\sqrt{\theta_W}\rho_W = \rho\,\theta + \frac{\sigma_{yy}}{2} - \frac{R_{yy}}{28\theta} - \frac{R}{120\theta} \tag{32}$$

The remaining 5 boundary conditions following from (29) and (31) with $V = v_x - v_W$ read

$$\sigma = -n_y \sqrt{\frac{2}{\pi\theta}} \frac{\chi}{2-\chi} \left(P\,V + \frac{1}{2} m_{xyy} + \frac{1}{5} q_x \right) \tag{33}$$

$$R_{xy} = n_y \sqrt{\frac{2}{\pi\theta}} \frac{\chi}{2-\chi} \left(P\,\theta\,V - \frac{1}{2}\theta\, m_{xyy} - \frac{11}{5}\theta\, q_x - P\,V^3 + 6P(\theta - \theta_W)V \right) \tag{34}$$

$$q_y = -n_y \sqrt{\frac{2}{\pi\theta}} \frac{\chi}{2-\chi} \left(2P(\theta - \theta_W) + \frac{5}{28} R_{yy} + \frac{1}{15} R + \frac{1}{2}\theta\,\sigma_{yy} - \frac{1}{2} P\,V^2 \right) \tag{35}$$

$$m_{yyy} = n_y \sqrt{\frac{2}{\pi\theta}} \frac{\chi}{2-\chi} \left(\frac{2}{5} P(\theta - \theta_W) - \frac{1}{14} R_{yy} + \frac{1}{75} R - \frac{7}{5}\theta\,\sigma_{yy} - \frac{3}{5} P\,V^2 \right) \tag{36}$$

$$m_{xxy} - m_{yzz} = -n_y \sqrt{\frac{2}{\pi\theta}} \frac{\chi}{2-\chi} \left(\frac{R_{xx} - R_{zz}}{14} + \theta(\sigma_{xx} - \sigma_{zz}) - P\,V^2 \right) \tag{37}$$

where we used a special ordering in correspondence with the coupling discussed below. Following the setting of Fig. 1 these boundary conditions have to hold on both sides of the channel with $n_y = \pm 1$ for lower (left) and upper (right) wall, respectively. Generalization to an arbitrary wall of a computational domain is straight forward. For the coupling of the quantities emphasis lies on linear terms. No linear terms lead to a coupling across all boundary conditions. The first two equations couple $\{v_x, \sigma, q_y, m_{xyy}, R_{xy}\}$ while the third and fourth equations couple $\{\theta, q_x, \sigma_{yy}, R_{yy}, m_{yyy}\}$. The last equation couples essentially $\{\sigma_{xx}, R_{xx}, m_{xxy}\}$.

The steady shear flow setting gives rise to one additional condition. In total, the mass between the walls should equal a given value M_0

$$\int_{-L/2}^{L/2} \rho(y)\, dy = M_0\,, \tag{38}$$

which can be viewed as generalized boundary condition. If v_y were allowed to be non-zero, the balance of mass would join the set of equations. In that case yet another boundary condition would be required and the condition (38) would be replaced by the boundary condition $v_y = 0$ on both walls. This also shows how the current shear flow setting can be extended to more generalized situations.

The boundary conditions (33)-(37) give explicit expressions for the relevant fluxes in terms of the non-flux quantities. The first condition can be identified as slip condition combining essentially the slip velocity V with the shear stress σ, i.e., the gradient of velocity in the NSF model. Similarly, the third equation gives the temperature jump $\theta - \theta_W$ in terms of the heat flux q_y, i.e., the gradient of temperature in NSF. The other equations represent jump conditions for higher order moments.

The accommodation coefficient χ appears as factor in each single equation. Already Grad [10] proposed to use different values of χ in each equation of (33)-(37), to reflect the fact that moment equations require a modification as indicated in Fig. 2. We argue that each flux is accommodated differently at the wall. Correspondingly, we substitute the factor $\chi/(2-\chi)$ in each equation by coefficients β_i where $i \in \{\sigma, R_{xy}, q_y, m_{yyy}, m_{xxy}\}$. The standard value of these coefficients is unity but they may be used as fitting parameters. The same strategy was used in [12] on a different set of boundary conditions.

3.5 Hypotheses

Investigating the matrix form of the R13 equation (91) reveals that in general $\det \mathbf{A}(\mathbf{U}) \neq 0$, hence, the system requires a full set of 13 boundary conditions in total. With (33)-(37) and (38) we have found 11 conditions. The question arises, how this lack of conditions should be handled?

3.5.1 Coherence of Boundary Conditions

Interestingly, it turns out that $\det \mathbf{A}(\mathbf{U}) \neq 0$ is not valid for all values of $\mathbf{U}$. When evaluating the linear case $\mathbf{A}(\mathbf{U}_0)$ (see below) we find a zero eigenvalue with multiplicity $\alpha = 2$. As soon as there are non-linear terms in the matrix this zero eigenvalue is lost. It follows that in the linear case all existing boundary conditions are sufficient and the R13-system with kinetic boundary conditions is well-posed.

This fact strengthens our confidence in the boundary conditions (33)-(37) and leads to the following hypothesis: *The transition from a process in the linear regime (small velocity/temperature differences) to a non-linear process should not change the number of boundary conditions.* That is, describing a non-linear process with R13 should not require more boundary conditions than describing a linear scenario. Otherwise, if this were not the case, the description could not be coherent, since smallest non-linear contributions in the equations would require an additional equation that needed to be dropped in the linear case. To be precise, the kernel of the zero eigenvalues of $\mathbf{A}(\mathbf{U}_0)$ imposes restrictions on the fields as described in Sec. 3.1 that must be viewed as supplements to the boundary conditions. In general, these kernel conditions would contradict any additional accommodation boundary conditions. For additional interpretation of the situation, see Sec. 5.4. The hypothesis concerns only the number of boundary conditions. Clearly, there will be non-linear contributions within the given conditions which are relevant or irrelevant depending on the non-linearity of the process.

3.5.2 High Order Equivalence

With the above hypothesis we render the boundary conditions (33)-(37) more fundamental than the system of equations. Indeed, we are now left with the question, how to modify the equations such that $\mathbf{A}(\mathbf{U})$ possesses a zero eigenvalue with multiplicity $\alpha = 2$ for *all values* of U, since only then the boundary conditions will be sufficient.

The reason for success of this approach lies in the fact that the equations allow more flexibility than the boundary conditions. We require the R13 equations to exhibit an asymptotic accuracy of fourth order as described in Sec. 2.2. It was shown by the order-of-magnitude approach in [28] that the equations may be altered in a certain way without influencing the asymptotic accuracy. This was also employed in [6] to stabilize the Burnett equations. Two systems with the same asymptotic accuracy will be called equivalent. The task is to find an equivalent system for (13)-(25) such that the resulting $\tilde{\mathbf{A}}(\mathbf{U})$ will allow the boundary conditions (33)-(37).

The kernel conditions of the transformed system correspond to bulk solutions. They bear relevance also for the original R13-equations and can be used as additional boundary conditions for the original system. An interpretation of the result is given later in Sec. 5.4.

The order-of-magnitude approach (see also [26]) assigns powers of Kn to every moment to

indicate the relevance with which the moments enter the asymptotic accuracy. In this sense σ_{ij} and q_i are first order quantities and m_{ijk} and $\hat{R}_{ij}$ are of second order. Furthermore, the R13 constitutive quantities m_{ijk} and $\hat{R}_{ij}$ enter the asymptotic accuracy with an additional factor Kn. Hence, the constitutive equations for m_{ijk} and $\hat{R}_{ij}$ may be altered by terms of $\mathcal{O}\left(Kn^3\right)$ without reducing the asymptotic accuracy. We will see below that this is sufficient to construct a system that suits the boundary conditions.

4 Linear Case

The linear case gives an enormous insight into the behavior and coupling of the R13 equation for shear flow, see also [32]. We linearize the equations around a given rest state at reference density, temperature and pressure

$$(\rho, \theta, p) = (\rho_R, \theta_R, p_R)\,, \tag{39}$$

all other variables vanish in the reference state.

4.1 Equations

After linearization, the equations uncover a striking simplicity by decomposing into three decoupled blocks. The first block describes the velocity part with the balances of v_x, σ, and q_x and constitutive equations for m_{xyy} and $\hat{R}_{xy}$, the second block describes the temperature part with balances of θ, q_y, and σ_{yy} with constitutive equations for $\hat{R}_{yy}$ and m_{yyy}. These two blocks have mathematically identical structures and the role of the variables could be directly exchanged. The third block is given by the balance of v_y, σ_{xx} with constitutive equations for m_{xxy}. This block is influenced by the temperature part.

To display the decoupling we sort the variable vector as

$$\mathbf{U} = \left\{ v_x, \sigma, q_x, m_{xyy}, R_{xy}, \theta, q_y, \sigma_{yy}, \hat{R}_{yy}, m_{yyy}, \rho, \sigma_{xx}, m_{xxy} \right\} \tag{40}$$

for which the linearized system can be written in the form $\mathbf{A}\partial_x\mathbf{U} = \mathbf{P}(\mathbf{U})$ with the matrix

$$\mathbf{A} = \left(\begin{array}{ccccc|ccccc|ccc}
0 & \frac{1}{\rho_R} & 0 & 0 & 0 & 0 & 0 & 0 & 0 & 0 & 0 & 0 & 0 \\
\mathrm{p}R & 0 & \frac{2}{5} & 1 & 0 & 0 & 0 & 0 & 0 & 0 & 0 & 0 & 0 \\
0 & \theta_R & 0 & 0 & \frac{1}{2} & 0 & 0 & 0 & 0 & 0 & 0 & 0 & 0 \\
0 & \frac{16}{15}\theta_R & 0 & 0 & 0 & 0 & 0 & 0 & 0 & 0 & 0 & 0 & 0 \\
0 & 0 & \frac{12}{5}\theta_R & 0 & 0 & 0 & 0 & 0 & 0 & 0 & 0 & 0 & 0 \\
\hline
0 & 0 & 0 & 0 & 0 & 0 & 1 & 0 & 0 & 0 & 0 & 0 & 0 \\
0 & 0 & 0 & 0 & 0 & \frac{5}{2}\mathrm{p}R & 0 & \theta_R & \frac{1}{2} & 0 & 0 & 0 & 0 \\
0 & 0 & 0 & 0 & 0 & 0 & \frac{6}{5} & 0 & 0 & 1 & 0 & 0 & 0 \\
0 & 0 & 0 & 0 & 0 & 0 & \frac{36}{5}\theta_R & 0 & 0 & 0 & 0 & 0 & 0 \\
0 & 0 & 0 & 0 & 0 & 0 & 0 & \frac{6}{5}\theta_R & 0 & 0 & 0 & 0 & 0 \\
\hline
0 & 0 & 0 & 0 & 0 & \rho_R & 0 & 1 & 0 & 0 & \theta_R & 0 & 0 \\
0 & 0 & 0 & 0 & 0 & 0 & \frac{2}{5} & 0 & 0 & 0 & 0 & 0 & 1 \\
0 & 0 & 0 & 0 & 0 & 0 & 0 & -\frac{4}{15}\theta_R & 0 & 0 & 0 & \frac{2}{3}\theta_R & 0
\end{array}\right) \tag{41}$$

where the different blocks are indicated by solid lines. The right hand side of the system reads

$$\mathbf{P}(\mathbf{U}) = -\frac{p_R}{\mu_R}\Big(-\tfrac{\mu_R}{p_R}F,\quad \sigma,\quad \tfrac{2}{3}q_x,\quad m_{xyy},\quad R_{xy},\quad 0,\quad \tfrac{2}{3}q_y,\quad \sigma_{yy},\quad R_{yy},\quad m_{yyy},\quad 0,\quad \sigma_{xx},\quad m_{xxy}\ \Big)^T. \tag{42}$$

Comparison of the first and second diagonal block in (41) shows the identical structure of the velocity and temperature parts. Both parts are governed dominantly by two classical variables, (v_x, σ) and (θ, q_y), respectively, which behave essentially in an intuitive way. In NSF the second variable is related to the gradient of the first. The third variable in both parts, q_x and σ_{yy}, respectively, is given by a seemingly classical variable which however plays an non-intuitive role. It represents a heat flux produced by a velocity shear and a normal stress due to temperature difference. Both are typical bulk effects in rarefied flows only triggered by boundary conditions. Through these variables the classical variables are coupled to the high order internal quantities, m_{xyy} and $\hat{R}_{xy}$, and, $\hat{R}_{yy}$ and m_{yyy}, respectively. From tensorial considerations the first block can be identified with mixed normal/tangential variables, while the second block couples the purely normal variables. The last block combines the density and purely tangential tensorial variables.

The matrix A has an eigenvalue $\lambda = 0$ with multiplicity $\alpha = 2$ and two corresponding left eigenvectors

$$\mathbf{x}_1 = \left(\frac{16}{15}p_R, 0, 0, -1, 0, 0, 0, 0, 0, 0, 0, 0, 0\right) \tag{43}$$

$$\mathbf{x}_2 = \left(0, 0, 0, 0, 0, \frac{36}{5}\theta_R, 0, 0, -1, 0, 0, 0, 0\right) \tag{44}$$

which satisfy $\mathbf{x}_{1,2} \cdot \mathbf{A} = 0$. These eigenvectors induce conditions on the variables which are given by

$$\mathbf{x}_1 \cdot \mathbf{P}(\mathbf{U}) = 0 \quad \Rightarrow \quad m_{xyy} = \frac{16}{15}\mu_R F\,, \tag{45}$$

$$\mathbf{x}_2 \cdot \mathbf{P}(\mathbf{U}) = 0 \quad \Rightarrow \quad \hat{R}_{yy} = 0\,. \tag{46}$$

These relations affect the velocity part through m_{xyy} and the temperature part through $\hat{R}_{yy}$. Both quantities can be inserted into the balance equations for σ and q_y, respectively, and hereafter be dropped from the variable vector. As a result, the fourth and ninth row and column of the matrix (41) can be dropped, as well as the fourth and ninth entry of $\mathbf{P}(\mathbf{U})$. The new system consists of two decoupled 4×4 blocks for the velocity and temperature parts, and the remaining three equations for density and σ_{xx}/m_{xxy} [32].

4.2 Boundary Conditions

For the linear case, the boundary condition (33)-(37) must be linearized as well, so that all terms non-linear in slip velocity V and temperature jump $\theta - \theta_W$ vanish. Factors depending on density, temperature and pressure are replaced by their reference values (39).

After elimination of m_{xyy} and R_{yy} the system fits seamlessly to the boundary conditions. The velocity part requires 4 boundary conditions and these are given by (33) and (34) on both sides of the channel. Similarly, for the temperature part (35) and (36) are used. Note, that the decoupling of the boundary conditions perfectly mimics the decoupling of the equations in the linear case.

The last two equations of the linear system, which involve σ_{xx} and m_{xxy}, can be solved after the temperature part for diagnostic purposes. These equations need two boundary conditions, which are given by (37) on both sides of the channel. Finally, the density can be computed by integrating the momentum balance for v_y and condition (38).

4.3 Velocity Part

As a reference we give the explicit equations for the velocity part in the linearized case. The variables are $\mathbf{U} = \{v_x, \sigma, q_x, R_{xy}\}$ and the system reads

$$\begin{pmatrix} 0 & \frac{1}{\rho_R} & 0 & 0 \\ p_R & 0 & \frac{2}{5} & 0 \\ 0 & \theta_R & 0 & \frac{1}{2} \\ 0 & 0 & \frac{12}{5}\theta_R & 0 \end{pmatrix} \begin{pmatrix} \partial_y v_x \\ \partial_y \sigma \\ \partial_y q_x \\ \partial_y R_{xy} \end{pmatrix} = \begin{pmatrix} F \\ -\frac{p_R}{\mu_R}\sigma \\ -\frac{2}{3}\frac{p_R}{\mu_R}q_x \\ -\frac{p_R}{\mu_R}R_{xy} \end{pmatrix} \tag{47}$$

while the boundary conditions on the lower and upper wall, index $(0,1)$, are given by

$$\sigma|_{0,1} = \pm\sqrt{\frac{2}{\pi\theta_R}}\frac{\chi}{2-\chi}\left(p_R\,(v_x - v_w) + \frac{8}{15}\mu_R F + \frac{1}{5}q_x\right)\Big|_{0,1}, \tag{48}$$

$$R_{xy}|_{0,1} = \pm\sqrt{\frac{2\theta_R}{\pi}}\frac{\chi}{2-\chi}\left(-p_R\,(v_x - v_w) + \frac{8}{15}\mu_R F + \frac{11}{5}q_x\right)\Big|_{0,1}. \tag{49}$$

The general analytical solution is easy to obtain but rather lengthy to write down. Thus, we omit it here, see [32] for special cases.

5 Nonlinear Case

When studying the non-linear case we consider first the force-less situation

$$F = 0. \tag{50}$$

The force will be added in Sec. 5.3. We tackle the non-linearity in two steps, first with the restriction of linear constitutive equations for m_{ijk} and R_{ij}, and after this fully non-linear.

5.1 Semi-Nonlinear

In this section the balance equations of momentum, energy, stress and heat flux are considered fully non-linear, while only the leading linear expression is kept in the constitutive equation (21)-(25). First, we simplify the balance equations for q_x and q_y by adding (14) times $\frac{\sigma}{\rho}\theta$ to (19) and (14) times $\frac{\sigma_{yy}}{\rho}\theta$ to (20). This eliminates the occurrence of the density gradient.

We start with the full variable vector (40); the system $A(U)\partial_y U = P(U)$ is now built from matrix and right hand side given by

$$\mathbf{A}\left(\mathbf{U}\right) = \tag{51}$$

$$\left(\begin{array}{ccccc|ccccc|ccc}
0 & \frac{1}{\rho} & 0 & 0 & 0 & 0 & 0 & 0 & 0 & 0 & 0 & 0 & 0 \\
p+\sigma_{yy} & 0 & \frac{2}{5} & 1 & 0 & 0 & 0 & 0 & 0 & 0 & 0 & 0 & 0 \\
\frac{7}{5}q_y+m_{xxy} & \theta-\frac{\sigma_{xx}}{\rho} & 0 & 0 & \frac{1}{2} & \frac{7}{2}\sigma & 0 & 0 & 0 & 0 & 0 & 0 & 0 \\
0 & \frac{16}{15}\theta & 0 & 0 & 0 & 0 & 0 & 0 & 0 & 0 & 0 & 0 & 0 \\
0 & 0 & \frac{12}{5}\theta & 0 & 0 & 0 & 0 & 0 & 0 & 0 & 0 & 0 & 0 \\
\hline
\sigma & 0 & 0 & 0 & 0 & 0 & 1 & 0 & 0 & 0 & 0 & 0 & 0 \\
\frac{2}{5}q_x+m_{xyy} & -\frac{\sigma}{\rho} & 0 & 0 & 0 & \frac{5}{2}p+\frac{7}{2}\sigma_{yy} & 0 & \theta & \frac{1}{2} & 0 & 0 & 0 & 0 \\
0 & 0 & 0 & 0 & 0 & 0 & \frac{6}{5} & 0 & 0 & 1 & 0 & 0 & 0 \\
0 & 0 & 0 & 0 & 0 & 0 & \frac{36}{5}\theta & 0 & 0 & 0 & 0 & 0 & 0 \\
0 & 0 & 0 & 0 & 0 & 0 & 0 & \frac{6}{5}\theta & 0 & 0 & 0 & 0 & 0 \\
\hline
0 & 0 & 0 & 0 & 0 & \rho & 0 & 1 & 0 & 0 & \theta & 0 & 0 \\
2\sigma & 0 & 0 & 0 & 0 & 0 & \frac{2}{5} & 0 & 0 & 0 & 0 & 0 & 1 \\
0 & 0 & 0 & 0 & 0 & 0 & 0 & -\frac{4}{15}\theta & 0 & 0 & 0 & \frac{2}{3}\theta & 0
\end{array}\right)$$

and

$$\mathbf{P}(\mathbf{U}) = -\frac{p}{\mu}\left(\ 0,\quad \sigma,\quad \tfrac{2}{3}q_x,\quad m_{xyy},\quad \hat{R}_{xy},\right.$$
$$\left.0,\quad \tfrac{2}{3}q_y,\quad \sigma_{yy},\quad \hat{R}_{yy},\quad m_{yyy},\quad 0,\quad \sigma_{xx},\quad m_{xxy}\ \right)^T. \tag{52}$$

The solid lines indicate the blocks known from the linear case. However, now there appear non-linear coupling terms and the velocity and temperature parts can no longer be solved independently. The major coupling is introduced through the dissipation term $\sigma\partial_y v_x$ in the energy equation (15). Further coupling is present in the balance equation for heat flux. Some non-linear contributions also enter the diagonal blocks themselves.

We proceed to eliminate some variables analogously to the linear case. The matrix $\mathbf{A}(\mathbf{U})$ again has the eigenvalue $\lambda = 0$ with multiplicity $\alpha = 2$, however, the eigenspace is only one-dimensional. We find

$$\mathbf{x}_1 = \left(\frac{16}{15}p, 0, 0, -1, 0, 0, 0, 0, 0, 0, 0, 0, 0\right) \tag{53}$$

satisfying $\mathbf{x}_1 \cdot \mathbf{A}(\mathbf{U}) = 0$. Evaluating this on the system we obtain

$$\mathbf{x}_1 \cdot \mathbf{P}\left(\mathbf{U}\right) = 0 \quad \Rightarrow \quad m_{xyy} = 0 \tag{54}$$

in agreement with the linear case and $F = 0$. This allows to eliminate m_{xyy} and drop the fourth row and column in $\mathbf{A}(\mathbf{U})$. This new reduced matrix still has an zero eigenvalue and a left-nullspace

$$\mathbf{x}_2 = \left(0, -\sigma, 0, \frac{1}{6}\frac{\sigma}{\theta}, p+\sigma_{yy}, 0, 0, -\frac{5}{36}\frac{p+\sigma_{yy}}{\theta}, 0, 0, 0, 0\right) \tag{55}$$

which can be used to calculate an expression for R_{yy}

$$\mathbf{x}_2 \cdot \mathbf{P}\left(\mathbf{U}\right) = 0 \quad \Rightarrow \quad R_{yy} = \frac{6}{5}\sigma\frac{R_{xy} - 6\theta\,\sigma}{p+\sigma_{yy}}. \tag{56}$$

Note, that this is a fully non-linear statement and it reduces to $R_{yy} = 0$, when in the linear case (46). Hence, the linear case is included.

The expression (56) can be used to eliminate R_{yy} from the equations and drop the ninth row and column from the matrix (51). The final system requires 11 boundary conditions given by the kinetic relations (33)-(37) on both sides of the channel and mass conservation (38) like in the linear case.

5.2 Nonlinear

As soon as any of the non-linear contributions of the constitutive equations (21)-(25) are included in the matrix $\mathbf{A}(\mathbf{U})$ its determinant becomes non-zero. In principle, this makes 13 boundary condition necessary. However, according to our hypothesis we reformulate the system such that as many boundary conditions are required as in the linear and semi-non-linear case.

To be precise, the equations (21)-(25) for $\{m_{xxy}, m_{yyy}, m_{xyy}, R_{xy}, R_{yy}\}$ need to be altered and all non-linear terms recast into algebraic form. These algebraic terms then move to the right hand side of the system into $\mathbf{P}(\mathbf{U})$, while the matrix $\mathbf{A}(\mathbf{U})$ will be the same as in (51). This transformation is possible since the change produces a system that still is of fourth order asymptotic accuracy.

As a first step we eliminate the density gradient from the equations for m_{ijk} and R_{ij} (21)-(25) by use of the momentum balance (14) $\frac{\theta}{\rho}\,\partial_y\rho = -\partial_y\theta - \frac{1}{\rho}\partial_y\sigma_{yy}$. Temperature and velocity gradients can be substituted by heat flux and stress

$$\mu\partial_y\theta = -\frac{4}{15}q_y^{(\mathrm{NSF})} = -\frac{4}{15}q_y + \mathcal{O}\left(Kn^2\right), \tag{57}$$

$$\mu\partial_y v_x = -\sigma^{(\mathrm{NSF})} \quad = -\sigma + \mathcal{O}\left(Kn^2\right), \tag{58}$$

which introduces an asymptotic accuracy error of $\mathcal{O}(Kn^2)$. However, these expressions are multiplied in the equations (21)-(25) by stress and heat flux, both first order quantities, thus the overall error to m_{ijk} and R_{ij} is $\mathcal{O}(Kn^3)$. This is sufficient for an asymptotically equivalent system, see Sec. 3.5.2. The remaining gradients of the normal stress σ_{yy} are of the form

$$\frac{\mu}{\rho}\frac{\sigma_{yy}}{p}\partial_y\sigma_{yy} = \mathcal{O}\left(Kn^3\right) \tag{59}$$

and may be dropped entirely without changing accuracy. Thus, the final equations which replace (21)-(25) are given by

$$-\frac{p}{\mu}\left(m_{xxy} + \frac{8}{225p}(2\sigma_{yy}q_y - 5\,\sigma_{xx}q_y - 12\sigma q_x)\right) = \frac{2}{3}\theta\,\partial_y\sigma_{xx} - \frac{4}{15}\theta\,\partial_y\sigma_{yy} \tag{60}$$

$$-\frac{p}{\mu}\left(m_{yyy} - \frac{8}{25p}(\sigma_{yy}\,q_y - \sigma\,q_x)\right) = \frac{6}{5}\theta\,\partial_y\sigma_{yy} \tag{61}$$

$$-\frac{p}{\mu}\left(m_{xyy} - \frac{32}{45p}\sigma\,q_y\right) = \frac{16}{15}\theta\,\partial_y\sigma \tag{62}$$

for m_{ijk} and

$$-\frac{p}{\mu}\left(\hat{R}_{xy}-\frac{32}{25p}q_xq_y-\frac{12}{7\rho}(\sigma_{xx}+\sigma_{yy})\sigma\right)=\frac{12}{5}\theta\,\partial_y q_x \tag{63}$$

$$-\frac{p}{\mu}\left(\hat{R}_{yy}-\frac{136}{25p}q_yq_y-\frac{36}{7\rho}\sigma^2\right)=\frac{36}{5}\theta\,\partial_y q_y \tag{64}$$

for R_{ij}. We note, that this transformation can also be performed on the full three-dimensional equations, as well as with the variants of R13 given in [26]. Note, that the steady energy balance is needed to eliminate density gradients. The influence of this fact needs to be studied in future.

The new algebraic terms change the right hand side of our system to

$$\begin{aligned}\mathbf{P}(\mathbf{U})=-\frac{p}{\mu}\Big(\;&0,\quad \sigma,\quad \tfrac{2}{3}q_x,\quad m_{xyy}-\tfrac{32}{45}\tfrac{\sigma\,q_y}{p},\quad \hat{R}_{xy}-\tfrac{32}{25}\tfrac{q_xq_y}{p}-\tfrac{12}{7}\tfrac{(\sigma_{xx}+\sigma_{yy})\sigma}{\rho},\\ &0,\quad \tfrac{2}{3}q_y,\quad \sigma_{yy},\quad \hat{R}_{yy}-\tfrac{136}{25}\tfrac{q_y^2}{p}-\tfrac{36}{7}\tfrac{\sigma^2}{\rho},\quad m_{yyy}-\tfrac{8}{25}\tfrac{\sigma_{yy}\,q_y-\sigma\,q_x}{p},\\ &0,\quad \sigma_{xx},\quad m_{xxy}+\tfrac{8}{225}\tfrac{2\sigma_{yy}q_y-5\,\sigma_{xx}q_y-12\sigma q_x}{p}\;\Big)^T\end{aligned} \tag{65}$$

while the matrix $\mathbf{A}$ is still given by (51). Hence, the null-space vector $\mathbf{x}_1$ is still the same, but now we find

$$\mathbf{x}_1\cdot\mathbf{P}\,(\mathbf{U})=0\quad\Rightarrow\quad m_{xyy}=\frac{32}{45}\frac{\sigma\,q_y}{p} \tag{66}$$

which shows a non-linear relation for m_{xyy}. Introducing this relation for m_{xyy} into the balance equation for σ (18)we obtain

$$(p+\sigma_{yy})\partial_y v_x+\frac{2}{5}\partial_y q_x+\frac{32}{45}\frac{q_y}{p}\partial_y\sigma\;+\frac{32}{45}\frac{\sigma}{p}\partial_y q_y=-\frac{p}{\mu}\sigma. \tag{67}$$

The expression containing the pressure gradient $\sigma\,q_y\partial_y p=-\sigma q_y\partial_y\sigma_{yy}$ (momentum balance) is of third order in Kn and is neglected in the above equation for σ. Using this modified balance equation for σ the variable m_{xyy} drops out of the system and, as before, the fourth row and column of the matrix can be deleted.

However, the new terms from the balance equation for σ change the resulting new matrix. Interestingly, we still find a null-space spanned by the vector

$$\mathbf{x}_2=\left(\frac{32}{45}\frac{q_y\sigma}{\theta},-\sigma,0,\frac{\sigma}{6\theta},p+\sigma_{yy}+\frac{32}{45}\frac{\sigma^2}{p},0,0,-\frac{5}{36}\frac{p+\sigma_{yy}}{\theta},0,0,0,0\right) \tag{68}$$

where expressions of third and higher order have been suppressed already. This null-vector yields

$$\mathbf{x}_2\cdot\mathbf{P}\,(\mathbf{U})=0\quad\Rightarrow\quad \hat{R}_{yy}=\frac{136}{25p}q_y^2-\frac{72}{35\rho}\sigma^2 \tag{69}$$

as expression for $\hat{R}_{yy}$ up to third order. Finally, we insert R_{yy} into the balance of q_y

$$\theta\partial_y\sigma_{yy}+(\frac{5}{2}p+\frac{7}{2}\sigma_{yy}-\frac{36}{35}\frac{\sigma^2}{p})\partial_y\theta-\frac{107}{35}\frac{\sigma}{\rho}\partial_y\sigma+\frac{136}{25}\frac{q_y}{p}\partial_y q_y+(m_{xyy}+\frac{2}{5}q_x)\partial_y v_x=-\frac{2p}{3\mu}q_y \tag{70}$$

and $\hat{R}_{yy}$ is eliminated from the system.

With the equations (67) and (70), and without m_{xyy} and $\hat{R}_{yy}$, the final fully non-linear system $\mathbf{A}(\mathbf{U})\partial_x\mathbf{U} = \mathbf{P}(\mathbf{U})$ is shown in Appendix A in (93) including the force F, see below. It is an 11×11 system which is complemented with the five boundary conditions (33)-(37) on both sides of the channel and the mass conservation (38).

5.3 With Force $F \neq 0$

We quickly consider the situation with external force

$$F \neq 0\,, \tag{71}$$

which was left out for simplicity above. The existence of a force changes the expression

$$\mathbf{x}_1 \cdot \mathbf{P}\,(\mathbf{U}) = 0 \quad \Rightarrow \quad m_{xyy} = \frac{32}{45p}\sigma\, q_y - \frac{16}{15}\mu\, F \tag{72}$$

for m_{xyy}. In contrast to the linear case, in this situation the term $\mu\, F$ gives a contribution when m_{xyy} is inserted the balance equation of σ. Since the viscosity is temperature-dependent (10) we obtain a temperature gradient in (67). This term again spoils the existence of a null-space to further reduce the system. Hence, we eliminate the gradient similar to the procedure before using $\partial_y\mu = \omega\frac{\mu}{\theta}\partial_y\theta = -\omega\frac{4}{15\theta}q_y + \mathcal{O}\left(Kn^2\right)$ and arrive at

$$(p+\sigma_{yy})\partial_y v_x + \frac{2}{5}\partial_y q_x + \frac{32}{45}\frac{q_y}{p}\partial_y\sigma \; + \frac{32}{45}\frac{\sigma}{p}\partial_y q_y = -\frac{p}{\mu}\sigma - \frac{64\omega}{225\theta}F\, q_y \tag{73}$$

as equation for σ. Here, the term with F is algebraic and moves to the right hand side. At this point we may continue to evaluate the null-space given by $\mathbf{x}_2$ as above and eliminate $\hat{R}_{yy}$.

Note, that the substitution of the temperature gradient is only possible if the force is small. Otherwise the change would not be third order in the Knudsen number. To be precise, in dimensionless form we need $F\,L/\theta_R \approx Kn$.

5.4 Interpretation

The major achievement of the calculations above are not the modified equations, but the discovery of the relations (69) and (72) inherently coupling the moment variables. These relations have a deeper meaning which becomes clear when studying larger moment systems.

5.4.1 Boundary Layer Reduction

In an infinite hierarchy applied to a boundary value problem all moment variables will exhibit boundary layers governed by the Knudsen number, except the two fluxes of the conservation variables, i.e., shear stress σ and heat flux q_y. Each boundary layer is formed from two moment variables, a variable of even degree in y and small tensor degree and a variable of higher tensor degree with odd degree. For the odd variable the kinetic boundary condition will furnish wall conditions on both sides which fixes the amplitude of the boundary layer. Away from the boundary the layer decays to the non-linear bulk solution determined by terms of lower differential

order in the equations. Interestingly, it seems that wherever a moment hierarchy is cut to obtain a finite system, there will always be some pairs of boundary layer variables that are separated. The lower variable is included while the higher variable is not considered. Also, since the higher variable drops out, the kinetic boundary condition is dismissed as well. We obtain a system in which even variables lack their partner and their boundary condition to produce a boundary layer. The modelling assumption is, that their boundary layer is somewhat thinner than the others and can be omitted. Still, due to lower order differential terms in the equations, these variables require some boundary conditions. Naturally, these variables are assumed to follow their bulk solution in the entire domain, hence also at the boundary.

In the case of R13 the even variables m_{xyy} and $\hat{R}_{yy}$ are missing a partner of higher tensor degree to produce a boundary layer. The other variables, e.g., q_x with $\hat{R}_{xy}$ and σ_{yy} with m_{yyy} form boundary layer pairs. The null space procedure described above provides a method to obtain the bulk solutions for the left over even variables. The bulk solutions are simply zero in the linear case, but have non-trivial non-linear contributions in general.

5.4.2 Other theories

The linearized original Grad 13 moment equations do not exhibit Knudsen layers, since the higher moments lack their partner. The requirement of consistency for boundary conditions for the linearized and non-linear equations leads directly to the statement that the non-linear bulk solutions of [30] together with jump and slip boundary conditions for temperature and velocity are the appropriate system to consider for 2nd order accuracy in the Knudsen number. Indeed, attempts to prescribe additional boundary conditions were not successful, and only lead to spurious non-linear boundary layers [34].

Similar problems are encountered by Gu and Emerson [12] who for the solution of the R13 equations prescribed a large number of kinetic boundary conditions on both walls. While they obey Grad's rule of choosing boundary conditions only for odd fluxes (see Sec. 3.4.2), they considered boundary conditions for higher fluxes that do not appear in the R13 equations. They solved only the non-linear equations, and their solutions show non-physical boundary layers close to the wall not observed in solutions of the Boltzmann equation. These must be attributed to the fact that they prescribe more boundary conditions than are required mathematically: The fully non-linear R13 equations for shear flow (26) require at most 13 boundary conditions, Gu and Emerson, however, prescribe more than 13 boundary conditions. Thus their problem is overdetermined, and they can produce results only by very careful adjustments of the accommodation coefficients.

6 Numerical Method

6.1 Shear Flow Setting

We consider the one-dimensional domain $y \in [-L/2, L/2]$ as depicted in Fig. 1. The simulation results in this paper are based on a numerical method formulated for the transformed system (93) in a straightforward way. This system is 11×11 with non-singular matrix and is complemented with the boundary conditions (33)-(37) at $y = -L/2$ and at $y = L/2$, as well as the total mass

conservation (38). The discretization is given by n point values

$$\mathbf{U}_i = \mathbf{U}\left(y_i\right), \qquad y_i = -L/2 + i\,\Delta y, \qquad \Delta y = \frac{L}{n+1} \tag{74}$$

such that y_0 and y_{n+1} are the boundary points. The values $\mathbf{U}_0$ and $\mathbf{U}_{n+1}$ will be first extrapolated from the interior, and some of them are then replaced by means of the boundary conditions.

As further reduction, the density is separated from the system and we consider it to be a system of non-linear equations for

$$\mathbf{U} = \left\{v_x, \sigma, q_x, R_{xy}, \theta, q_y, \sigma_{yy}, m_{yyy}, \sigma_{xx}, m_{xxy}\right\}, \tag{75}$$

which will be solved by iterative solutions of linear systems. The density appears in the matrix and on the right hand side as a parameter and has to be recomputed in each iteration from the integrated momentum balance

$$\rho = \frac{P_0 - \sigma_{yy}}{\theta} \tag{76}$$

where the constant P_0 follows from the mass conservation (38). We used $M_0 = 1$ and trapezoidal rule to compute P_0 from the current values θ and σ_{yy} within each iteration.

The right hand side $P(U)$ is split into a matrix operation and the inhomogeneous part in the form

$$\mathbf{P}\left(\mathbf{U}\right) = -\widetilde{\mathbf{P}}\left(\mathbf{U}\right)\mathbf{U} + \mathbf{P}_{\text{inh}} \tag{77}$$

where $\widetilde{\mathbf{P}}\left(\mathbf{U}\right)$ and $\mathbf{P}_{\text{inh}}$ are given in Appendix B in (95)/(96). The inhomogeneous part contains only the external force. With this, the system $\mathbf{A}(\mathbf{U})\partial_y\mathbf{U} = \mathbf{P}(\mathbf{U})$ is discretized using central differences

$$\frac{1}{2\Delta y}\left(\mathbf{A}(\mathbf{U}_i^{(k)})\mathbf{U}_{i+1}^{(k+1)} - \mathbf{A}(\mathbf{U}_i^{(k)})\mathbf{U}_{i-1}^{(k+1)}\right) + \widetilde{\mathbf{P}}(\mathbf{U}_i^{(k)})\mathbf{U}_i^{(k+1)} = \mathbf{P}_{\text{inh}} \qquad 1 \le i \le n \tag{78}$$

at all interior points. The superscripts (k) indicates the iterations. The boundary conditions have to be built into the boundary values $\mathbf{U}_0$ and $\mathbf{U}_{n+1}$. First, all values are constructed from the interior points

$$\mathbf{U}_0 = 2\mathbf{U}_1 - \mathbf{U}_2, \qquad \mathbf{U}_{n+1} = 2\mathbf{U}_n - \mathbf{U}_{n-1} \tag{79}$$

using linear extrapolation. The boundary conditions are incorporated based on these values. We rewrite the boundary conditions (33)-(37) for the entire variable vector in the form

$$\mathbf{U} = \mathbf{B}(\mathbf{U})\mathbf{U} + \mathbf{B}_{\text{inh,p}}(\mathbf{U}) \tag{80}$$

where $\mathbf{B}(\mathbf{U})$ and $\mathbf{B}_{\text{inh,p}}(\mathbf{U})$ can be found in Appendix B in (98)/(99). The inhomogeneous part $\mathbf{B}_{\text{inh,p}}\left(\mathbf{U}\right)$ with $p \in \{0,1\}$ contains the wall values $\theta_W^{(0,1)}$ and $v_W^{(0,1)}$, as well as the non-linear expressions of slip velocity and temperature jump. In (80) only the rows for $\{\sigma, R_{xy}, q_y, m_{yyy}, m_{xxy}\}$ give boundary conditions, while the rows for $\{v_x, q_x, \theta, \sigma_{yy}, \sigma_{xx}\}$ give identities. Relation (80) is

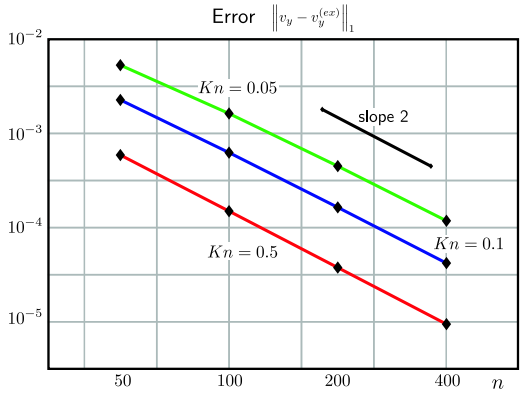

Figure 3: Empirical convergence of the proposed numerical method. Velocity of the linear R13 equations compared with exact solution for different grids and Knudsen numbers.

now evaluated on the extrapolated values (79) and inserted into (78). We obtain for $i = 1$

$$\frac{1}{2\Delta y}\mathbf{A}(\mathbf{U}_1^{(k)})\left(\mathbf{I}+\mathbf{B}(\mathbf{U}_1^{(k)})\right)\mathbf{U}_2^{(k+1)} + \left(\widetilde{\mathbf{P}}(\mathbf{U}_1^{(k)}) - \frac{1}{\Delta y}\mathbf{A}(\mathbf{U}_1^{(k)})\mathbf{B}(\mathbf{U}_1^{(k)})\right)\mathbf{U}_1^{(k+1)} = \mathbf{P}_{\text{inh}} + \frac{1}{2\Delta y}\mathbf{A}(\mathbf{U}_1^{(k)})\mathbf{B}_{\text{inh},0}(\mathbf{U}_1^{(k)}) \quad (81)$$

and for $i = n$

$$-\frac{1}{2\Delta y}\mathbf{A}(\mathbf{U}_n^{(k)})\left(\mathbf{I}+\mathbf{B}^*(\mathbf{U}_n^{(k)})\right)\mathbf{U}_{n-1}^{(k+1)} + \left(\widetilde{\mathbf{P}}(\mathbf{U}_n^{(k)}) + \frac{1}{\Delta y}\mathbf{A}(\mathbf{U}_n^{(k)})\mathbf{B}^*(\mathbf{U}_n^{(k)})\right)\mathbf{U}_n^{(k+1)} = \mathbf{P}_{\text{inh}} - \frac{1}{2\Delta y}\mathbf{A}(\mathbf{U}_n^{(k)})\mathbf{B}^*_{\text{inh},1}(\mathbf{U}_n^{(k)}) \quad (82)$$

as replacement for (78). For simplicity we use $\mathbf{U}_1$ and $\mathbf{U}_n$ in the evaluation of $\mathbf{B}$ instead of $\mathbf{U}_0$ and $\mathbf{U}_{n+1}$ with no serious loss of accuracy.

The form (80) is valid for the left wall. When using it for the right wall sign changes occur in the variables indicated by $\mathbf{B}^*$ and $\mathbf{B}^*_{\text{inh},1}$. The functions for the right wall are given by

$$\mathbf{B}^*(\mathbf{U}) = \mathbf{Q}\mathbf{B}(\mathbf{U})\mathbf{Q}, \quad \mathbf{B}^*_{\text{inh},1}(\mathbf{U}) = \mathbf{Q}\mathbf{B}_{\text{inh},1}(\mathbf{U}). \quad (83)$$

with the use of the transformation matrix $\mathbf{Q} = diag\,(1,-1,1,-1,1,-1,1,-1,1,-1)$.

Combining all discrete values $\mathbf{X}^{(k)} = \{U_i^{(k)}\}_{1\le i\le n}$ we obtain a system in the form

$$\mathcal{A}\left(\mathbf{X}^{(k)}\right)\cdot\mathbf{X}^{(k+1)} = \mathbf{Y}\left(\mathbf{X}^{(k)}\right) \quad (84)$$

with some block matrix $\mathcal{A}(\mathbf{X})$ which is solved iteratively. As start value $\mathbf{X}^{(0)}$ of the iteration we choose a reference equilibrium. Hence, the linear R13-system is solved in the first iteration. The stopping criteria is chosen to be

$$\left\|\mathbf{X}^{(k+1)} - \mathbf{X}^{(k)}\right\| \le \text{tol} \quad (85)$$

in some L^1-type norm. The whole procedure was implemented and used in the algebra-software Mathematica.

In the linear case, the exact solution of the R13 equations is easily obtained, see Sec. 4.3. Based on the exact solution an empirical study of the convergence order of the numerical method shows clear second order of the numerical error. Bigger Knudsen numbers show smaller errors. Note, that in this case non-linear iterations were not conducted. In the non-linear case, the numerical method requires 3-5 iterations for convergence.

6.2 General Setting

The above numerical method was tailored for the transformed system (93) with non-singular matrix. The variables m_{xyy}, $\hat{R}_{yy}$ and ρ have explicitly been eliminated which resulted in a stable solution.

In more general settings we have to deal with fully two-dimensional and/or unsteady situations where the elimination would not be possible. While the details have not been examined yet, we propose to use the internal relations

$$\hat{R}_{yy} = \frac{136}{25p} q_y^2 - \frac{72}{35\rho}\sigma^2 \tag{86}$$

$$m_{xyy} = \frac{32}{45p}\sigma\, q_y - \frac{16}{15}\mu\, F \tag{87}$$

obtained from the null-space conditions as boundary conditions in addition to the kinetic relations (33)-(37). Furthermore, the mass conservation condition (38) can be substituted with $v_y = 0$ on the boundary if the velocity v_y is considered part of the variable set.

The implementation and investigation of this approach in a general setting is left for future work.

7 Results

In this section we will discuss the results obtained with the new method for channel flows and compare some of these to values obtained from Direct-Simulation-Monte-Carlo (DSMC) methods and direct solutions of the Boltzmann equation. In these calculations we use different modified accommodation coefficients $\tilde{\beta}_i = \frac{\chi_i}{2-\chi_i} = \sqrt{\frac{\pi\theta}{2}}\beta_i$, see (97) and (100) in the appendix, for each moment boundary condition in order to match the DSMC and Boltzmann results. We also allow these coefficients to vary with Knudsen number, see Table 1, such that an overall agreement with DSMC is achieved. The influence and relevance of these coefficients is discussed in Sec. 7.3 below.

The computational domain $y \in [-0.5, 0.5]$ was discretized with $N = 200$ points.

7.1 Poiseuille Flow

Poiseuille flow is given by acceleration-driven channel flow with walls at rest. The channel is considered to be infinitely long such that a full velocity profile has developed from the viscous boundary layers. The given acceleration can be interpreted as a homogeneous pressure gradient.

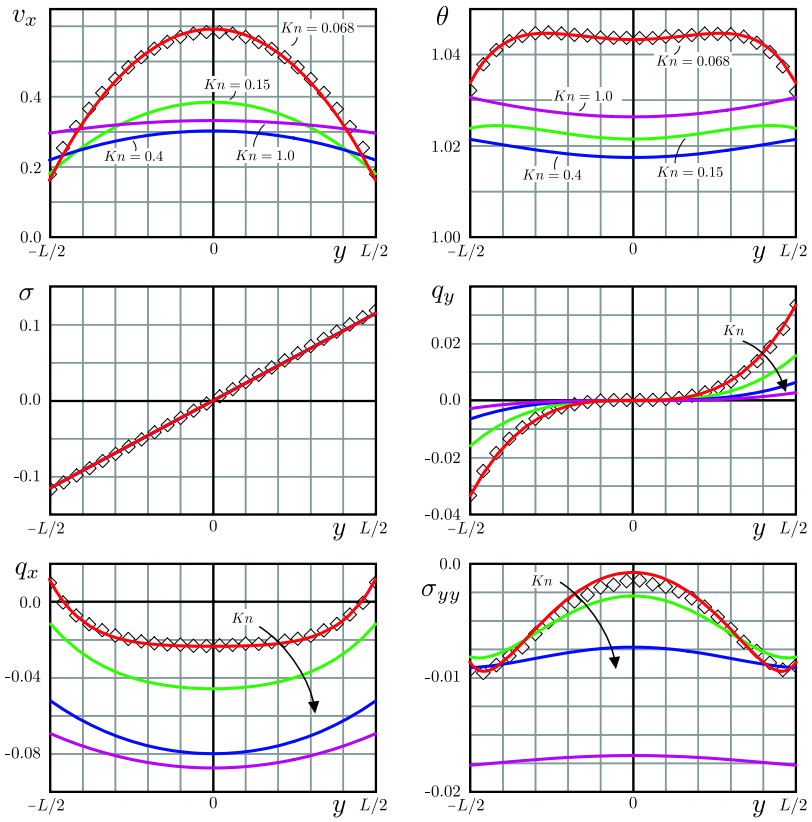

Figure 4: Accelaration-driven channel flow with dimensionless force $F = 0.23$ for different Knudsen numbers $Kn = 0.068$, 0.15, 0.4, 1.0. The result for $Kn = 0.068$ is compared to the DSMC results of [40] (symbols).

We solve the R13-system in the form (93) with kinetic boundary conditions (97) and $v_W^{(0,1)} = 0$, $\theta_W^{(0,1)} = 1$ for various Knudsen numbers with a dimensionless acceleration force fixed at $F = 0.23$ and viscosity exponent $\omega = 0.5$. These values are chosen such that a Knudsen number $Kn = 0.068$ reproduces the case of Poiseuille flow calculated in [40] (see also [39]) by DSMC. We also calculate the cases $Kn = 0.15$, 0.4, 1.0.

Fig. 4 displays the results for all Knudsen numbers together with the DSMC solution for $Kn = 0.068$. A good match with the DSMC result is obtained with accommodation coefficients given in Table 1. The figure shows the conservation variables velocity and temperature, their fluxes stress σ and heat flux q_y, as well as the rarefaction variables tangential heat flux q_x and normal stress σ_{yy}. All variables are reproduced as smooth curves without any tendencies to oscillate even when the grid is refined. Higher Knudsen numbers show stronger non-equilibrium as indicated by larger magnitudes of q_x and σ_{yy}. Interestingly, the temperature profile starts to invert for higher Knudsen numbers. This has still to be confirmed by DSMC calculations.

The rarefied flow through a channel is known to exhibit a paradoxical behavior known as Knudsen paradox, [15]. When reducing the Knudsen number in the experiment the normalized

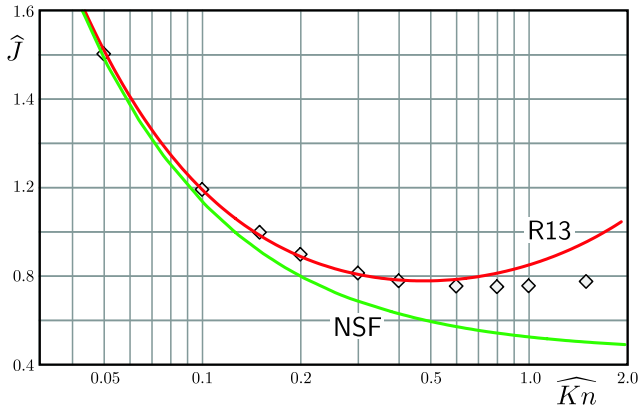

Figure5: Normalized mass flux through channel in the acceleration-driven case as a function of Knudsen number. Comparison between direct linear Boltzmann solution (symbols), R13 with new boundary model and Navier-Stokes-Fourier.

flow type	Kn-number	$\tilde{\beta}_1$	$\tilde{\beta}_2$	$\tilde{\beta}_3$	$\tilde{\beta}_4$	$\tilde{\beta}_5$
Poiseuille	0.068	0.9	0.35	0.9	0.5	1.0
Couette	0.1	0.9	0.4	0.92	0.6	1.0
	0.25	0.92	0.6	1.05	0.6	1.0
	0.5	1.05	0.8	1.35	0.7	1.0

Table 1: Modified accommodation coefficients $\tilde{\beta}_i$ used in the different simulations of Poiseuille and Couette flows with R13. These values give relatively good matching with DSMC data. The influence of the accommodation coefficients is discussed in Sec. 7.3.

mass flow rate

$$J = \int_{-1/2}^{1/2} v(y)\, dy \tag{88}$$

through the channel reaches a minimum and afterwards starts to increase for larger Knudsen numbers. Intuitively one would expect a decreasing mass flow for a smaller channel, but at a certain scale the friction inside the gas becomes so small that the growing slip velocity at the wall dominates the mass flow. This can also be observed in the results of the R13-system in Fig. 4. The velocity profile becomes flatter, but the slip increases and the velocity curve for $Kn = 1.0$ lies above the curve of $Kn = 0.4$.

In [22] the mass flow rate has been calculated based on the linearized Boltzmann equation. After correctly scaling the Knudsen number and the mass flow we compare the mass flow of the R13 results with those of [22] and Navier-Stokes-Fourier in Fig. 5. The classical theory of Navier-Stokes-Fourier fails to describe the Knudsen minimum. The mass flow for R13 follows the Boltzmann result fairly accurate until $Kn \lesssim 1.0$ and then lifts off too quickly. At these high Knudsen numbers the assumptions of the theory are not valid anymore. However, at lower Knudsen numbers the R13 systems demonstrates its ability to simulate micro-flows efficiently

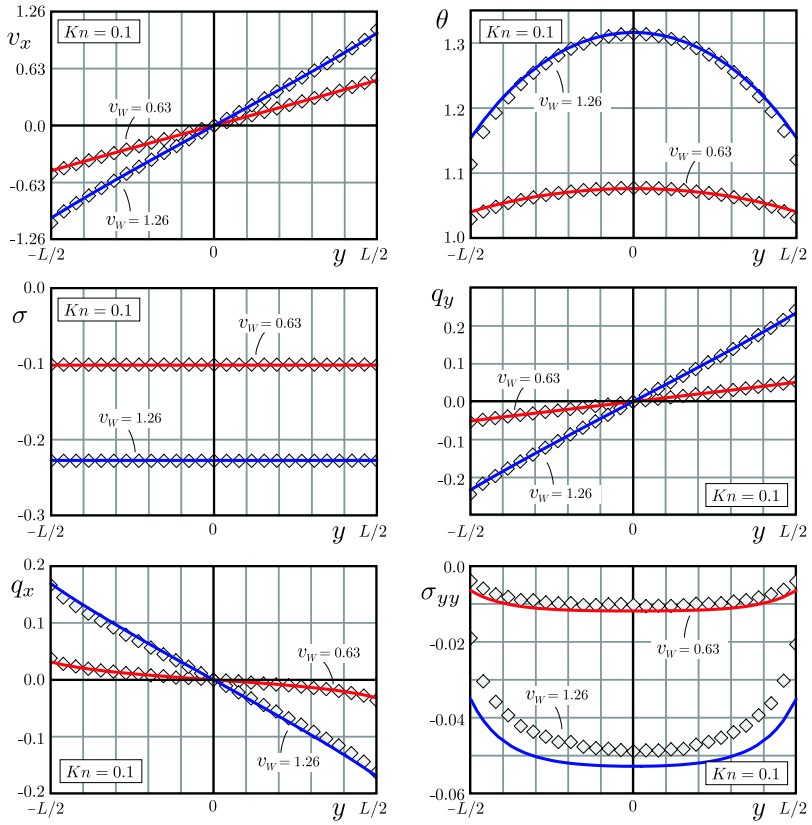

Figure 6: Symmetric shear flow (Couette flow) between two plates (left and right) at $Kn = 0.1$ for two different velocities of the walls. Comparison of R13 (lines) with DSMC (symbols).

and accurately.

7.2 Couette Flow

Typically, a channel flow where one wall is kept at rest while the other is moving is referred to as plane Couette flow. For symmetry reasons this setting corresponds to a channel flow where both walls move in opposite directions with identical speeds. Again, we solve the R13-system in the form (93) with kinetic boundary conditions (97). We choose $v_W^{(0)} = -v_W^{(1)}$ and $\theta_W^{(0,1)} = 1$ with two different choices for the dimensionless upper wall velocity $v_W^{(1)} = 0.63$ and $v_W^{(1)} = 1.26$. The Knudsen numbers considered are $Kn = 0.1$, 0.25, 0.5. For all these cases we compare with DSMC results produced in [34]. The viscosity exponent is $\omega = 1.0$.

For each Knudsen number the accommodation coefficients have been slightly modified for a good agreement according to Table 1. However, the same boundary conditions, and thus the same accommodation coefficients, have been used for different velocity cases. Interestingly, higher Knudsen numbers require slightly higher accommodation coefficients.

The simulation results for $Kn = 0.1$, 0.25, 0.5 are shown in Fig. 6, 7 and 8, respectively. As

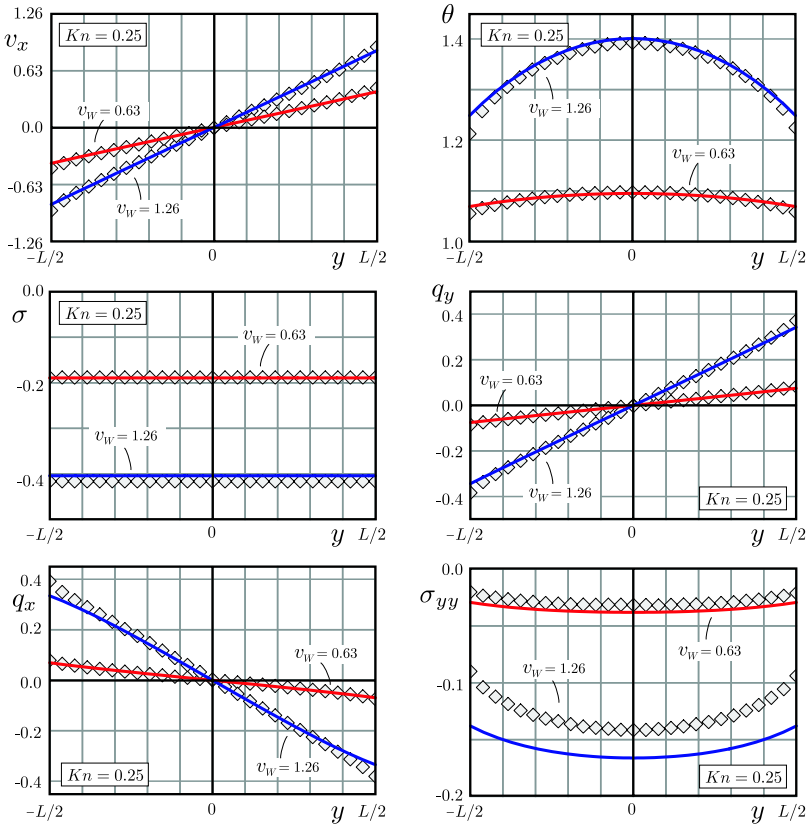

Figure 7: Symmetric shear flow (Couette flow) between two plates (left and right) at $Kn = 0.25$ for two different velocities of the walls. Comparison of R13 (lines) with DSMC (symbols).

before, we show the variables velocity and temperature with their fluxes stress σ and heat flux q_y and the rarefaction variables tangential heat flux q_x, and normal stress σ_{yy}. Both for higher velocities and higher Knudsen numbers the agreement between R13 and DSMC is weaker, but still acceptable, especially so for velocity and temperature. There might be a systematic error in the normal stress σ_{yy} since it shows a consistently larger error than the other fields.

We emphasize that our theory of boundary conditions leads to a smooth transition between linear and non-linear settings, and that only as many boundary conditions are prescribed as mathematically required. In particular this guarantees that conservation of energy and momentum is fulfilled for *all* values of the individual accommodation coefficients β_i, and that no spurious non-linear boundary layers appear. These features distinguish the present theory of boundary conditions from earlier attempts, e.g., [12], [34], where the prescription of too many boundary conditions lead to problems with conservation laws, and to spurious (non-linear) boundary layers.

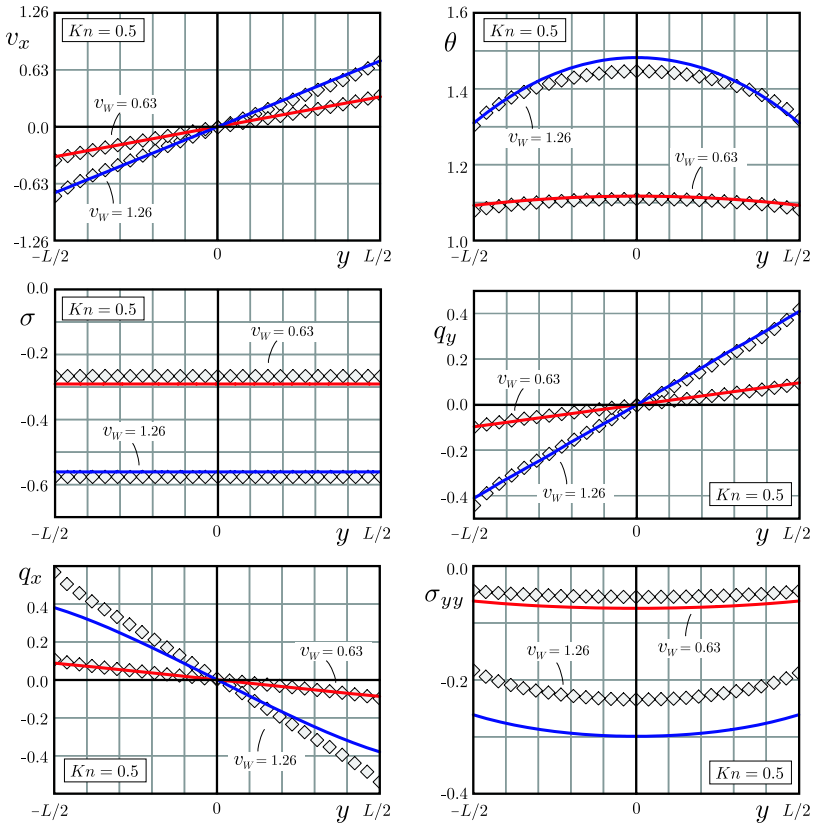

Figure 8: Symmetric shear flow (Couette flow) between two plates (left and right) at $Kn = 0.5$ for two different velocities of the walls. Comparison of R13 (lines) with DSMC (symbols).

7.3 Discussion of Accommodation Coefficients

Most simulations based on DSMC or direct Boltzmann solvers use the accommodation model (28) as boundary condition for the distribution function. However, the reduction of this model to boundary conditions for continuum equations has to be handled with caution. Already in the case of NSF it is known that the slip and jump boundary conditions have to be modified with artificial coefficients, see [7] or [26]. The reason for this correction is the lack of Knudsen layers in NSF. Similarly, the R13 equations are not able to describe the Knudsen layer completely due to the lack of sub layer contributions from higher moments, see [27] and Fig. 2. Hence, we expect the boundary conditions to be modified. The natural choice suggested by the structure of the equations (33)-(37) is to use different accommodation coefficients χ_i for different moments, i.e., fluxes. This was already suggested by Grad in [11]. To some extend, this modification can be viewed as generalization of the kinetic accommodation model, since one single parameter χ is certainly not enough to describe a general wall.

The physical and mathematical derivation of accommodation coefficients for moments remains open. A first hint is given in [32] where a phenomenological model of the wall lead to

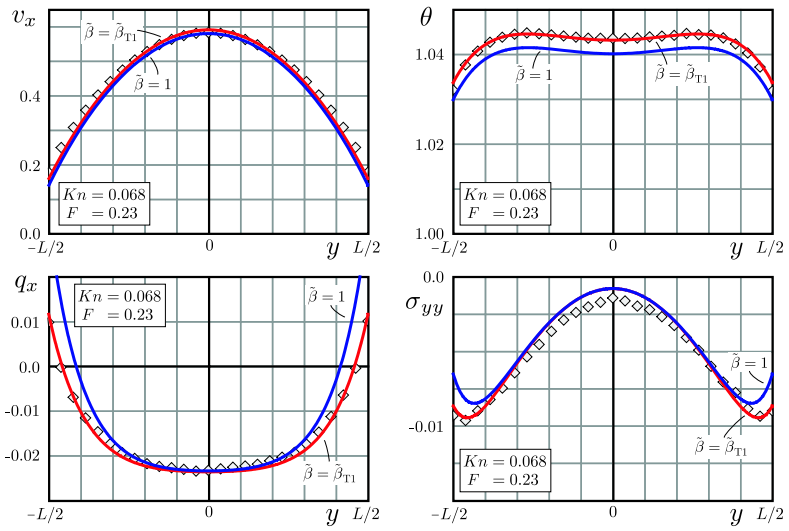

Figure 9: Comparison of the result for Poiseuille flow at $Kn = 0.068$ with different setting of the modified accommodation coefficients $\tilde{\beta}_i$. The values $\tilde{\beta}_{\mathrm{T1}}$ are given in Table 1, while the result with $\tilde{\beta} = 1$ sets all $\tilde{\beta}_i$ to unity.

boundary conditions structurally equivalent to (33)-(37) but with general positive coefficients in place of $\chi/(2-\chi) = \tilde{\beta}$. This result encourages us to modify $\tilde{\beta}_i$ in a more general way and also allow $\tilde{\beta}_i > 1$ in order to reproduce the DSMC result. Of course, the final theory should provide values for $\tilde{\beta}_i$ with minimal fitting and should by applicable in the general setting. This theory is out of scope of this paper. Here, we only give values for $\tilde{\beta}_i$ that produce good agreement and discuss the general influence of $\tilde{\beta}_i$ on the result.

If we restrict our focus to the fundamental shear flow variables $\{v_x, \sigma, q_x, \theta, q_y, \sigma_{yy}\}$ the qualitative influence of the $\tilde{\beta}_i$ on the solution is surprisingly simple. The main behavior in the vicinity of $\tilde{\beta}_i = 1$ is the following: The temperature jump coefficient $\tilde{\beta}_3$ influences only the temperature profile and has little to no effect on the rest of the variables. The profile is shifted upwards if $\tilde{\beta}_3$ is reduced and vice versa. The slip coefficient $\tilde{\beta}_1$ shifts the profiles of velocity and temperature simultaneously. If $\tilde{\beta}_1$ is decreasing the velocity profile is shifted upwards, while the temperature goes downwards. The coefficients $\beta_{2,4}$ are jump coefficients for the parallel heat flux and the normal stress, and both coefficients act independently on their variable. If increased, they increase the amplitude of the Knudsen layer of the respective variable.

We present two figures in which the quantitative difference in the solution can be studied when the $\tilde{\beta}_i$ are changing. The results found with the values for $\tilde{\beta}_i$ given in Table 1 are compared with the case $\tilde{\beta}_i = 1$. Fig. 9 shows the case of Poiseuille flow at $Kn = 0.068$. The values of $\tilde{\beta}_i$ in Table 1 are all below unity. The figure does not show shear stress and normal heat flux, since the solution curves exhibit virtually no differences. Most pronounced is the overestimation of the amplitude of the Knudsen layer in q_x and σ_{yy} due to the increase of $\tilde{\beta}_{2,4}$. Also, $\tilde{\beta}_3 = 1$ gives a too low temperature. Overall, the model shows a very stable behavior.

Fig. 10 shows the case of Couette flow at $Kn = 0.5$ and $v_W = 0.63$. Again, the case $\tilde{\beta}_i = 1$ is compared to the result based on the values in Table 1. As above, the normal heat flux shows

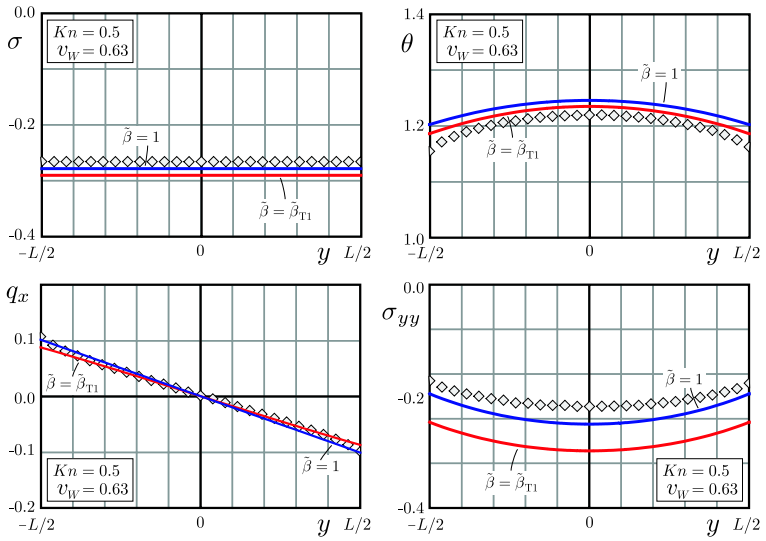

Figure 10: Comparison of the result for Couette flow at $Kn = 0.5$ and $v_W = 0.63$ with different setting of the modified accommodation coefficients $\tilde{\beta}_i$. The values $\tilde{\beta}_{\mathrm{T1}}$ are given in Table 1, while the result with $\tilde{\beta} = 1$ sets all $\tilde{\beta}_i$ to unity.

no difference, but this time the shear stress deviates more than the velocity profile. Thus, the figure shows shear stress, temperature, parallel heat flux and normal stress. The values of β_i in Table 1 have been chosen such that the temperature profile is matched and q_x exhibits the correct slope in the middle. Clearly, there is a trade-off between shear stress, temperature, and normal stress. The case $Kn = 0.5$ with $v_W = 0.63$ is a severe test at the of the validity of the equations and it is no surprise that difficulties arise. For a better judgement also comparisons to other DSMC data or Boltzmann solutions should be performed.

8 Conclusion

This paper presented a rigorous approach to boundary conditions for moment equations in kinetic theory based on mathematical and physical requirements. As basic set of equations the regularized 13-moment-system (R13) have been considered, while most of the findings can be generalized to other systems. Shear flow between two walls served as generic model for micro-flow simulations. We demonstrated that the boundary conditions that follow from kinetic accommodation models for the odd flux variables (five conditions on the wall for σ, R_{xy}, q_y, m_{yyy}, and m_{xxy}) are sufficient for both the linear and non-linear R13 equations. This agrees with our hypothesis that the number of boundary conditions should not change when moving from linear to non-linear equations.

However, to achieve this, the equations have to be transformed and the transformed system provides additional internal relations that may be considered as additional boundary conditions. The transformation was possible by adding expressions that are of high order in Knudsen number such that the overall asymptotic accuracy with respect to Boltzmann's equation does not change.

The additional internal relations represent the bulk solutions of certain moments that fail to produce a boundary layer due to a finite set of variables.

Once the boundary conditions have been found, the formulation of a numerical method was done in a straight forward way. Various examples for shear flow of Couette- and Poiseuille-type demonstrate the usefulness of the approach. From a physical point of view, additional modelling of specific accommodation coefficients is required for more accurate results.

Acknowledgement: MT: Support through the EURYI award of the European Science Foundation (ESF) is gratefully acknowledged. HS: Support by the Natural Sciences and Engineering Research Council (NSERC) is gratefully acknowledged. The paper was written during my stay as Gastprofessor at ETH Zürich, and I like to thank Prof. H.C. Öttinger and his group at the Institute for Polymer Physics for their kind hospitality.

A Matrix Formulation

A.1 Original System

The system (13)-(25) can be written in matrix form

$$\mathbf{A}\left(\mathbf{U}\right)\,\partial_y \mathbf{U} = \mathbf{P}\left(\mathbf{U}\right). \tag{89}$$

Here, we use the special physical grouping of the variable vector

$$\mathbf{U} = \{v_x, \sigma, q_x, m_{xyy}, R_{xy}, \theta, q_y, \sigma_{yy}, R_{yy}, m_{yyy}, \rho, \sigma_{xx}, m_{xxy}\} \tag{90}$$

which is in accordance with the decoupling observed in the linear case (41). The original fully non-linear system is given by

$$\left(\begin{array}{c} -\frac{\mu}{p}F \\ \sigma \\ \frac{2}{3}q_x \\ m_{xyy} \\ \hat{R}_{xy} \\ \hline 0 \\ \frac{2}{3}q_y \\ \sigma_{yy} \\ \hat{R}_{yy} \\ m_{yyy} \\ \hline 0 \\ \sigma_{xx} \\ m_{xxy} \end{array}\right) = -\frac{p}{\mu} \left(\begin{array}{c} \partial_y v_x \\ \partial_y \sigma \\ \partial_y q_x \\ \partial_y m_{xyy} \\ \partial_y \hat{R}_{xy} \\ \hline \partial_y \theta \\ \partial_y q_y \\ \partial_y \sigma_{yy} \\ \partial_y \hat{R}_{yy} \\ \partial_y m_{yyy} \\ \hline \partial_y \rho \\ \partial_y \sigma_{xx} \\ \partial_y m_{xxy} \end{array}\right)$$

$$\left(\begin{array}{ccccccccccccc} 0 & \frac{1}{\rho} & 0 & 0 & 0 & 0 & 0 & 0 & 0 & 0 & 0 & 0 & 0 \\ p+\sigma_{yy} & 0 & \frac{2}{5} & 1 & 0 & 0 & 0 & 0 & 0 & 0 & 0 & 0 & 0 \\ \frac{7}{5}q_y+m_{xxy} & \theta-\frac{\sigma_{xx}}{\rho} & 0 & 0 & \frac{1}{2} & 0 & 0 & 0 & 0 & 0 & 0 & 0 & 0 \\ \frac{32}{75}q_y & \frac{16}{15}\theta & 0 & 0 & 0 & -\frac{16}{15}\theta\frac{\sigma}{\rho} & 0 & 0 & 0 & 0 & 0 & 0 & 0 \\ \frac{12}{7}\theta(\sigma_{xx}+\sigma_{yy}) & 0 & \frac{12}{5}\theta & 0 & 0 & -\frac{12}{5}\theta\frac{q_x}{\rho} & 0 & 0 & 0 & 0 & 0 & 0 & 0 \\ \hline \sigma & 0 & 0 & 0 & 0 & 0 & 1 & 0 & 0 & 0 & 0 & 0 & 0 \\ \frac{2}{5}q_x+m_{xyy} & -\frac{\sigma}{\rho} & 0 & 0 & 0 & \frac{5}{2}(p+\sigma_{yy}) & 0 & \theta-\frac{\sigma_{yy}}{\rho} & \frac{1}{2} & 0 & 0 & 0 & 0 \\ 0 & 0 & 0 & 0 & 0 & 0 & \frac{6}{5} & 0 & 0 & 1 & 0 & 0 & 0 \\ \frac{22}{7}\theta\,\sigma & 0 & 0 & 0 & 0 & \frac{66}{5}q_y & \frac{36}{5}\theta & 0 & 0 & 0 & 0 & 0 & 0 \\ -\frac{8}{25}q_x & 0 & 0 & 0 & 0 & 0 & 0 & \frac{6}{5}\theta & 0 & 0 & 0 & 0 & 0 \\ \hline 0 & 0 & 0 & 0 & 0 & 0 & \rho & 0 & 1 & 0 & 0 & 0 & 0 \\ 2\sigma & 0 & 0 & 0 & 0 & 0 & 0 & \frac{2}{5} & 0 & 0 & 0 & 1 & 0 \\ 0 & 0 & 0 & 0 & 0 & 0 & 0 & 0 & -\frac{4}{15}\theta & 0 & 0 & 0 & \frac{2}{3}\theta \\ \hline 0 & 0 & 0 & 0 & 0 & -\frac{12}{5}\theta\frac{q_x}{\rho} & 0 & -\frac{6}{5}\theta\frac{\sigma}{\rho} & 0 & 0 & \theta & 0 & 0 \\ 0 & 0 & 0 & 0 & 0 & -\frac{16}{15}\theta\frac{\sigma}{\rho} & 0 & -\frac{36}{5}\theta\frac{q_y}{\rho} & 0 & 0 & 0 & 0 & 0 \\ -\frac{\mu}{p}F & \sigma & \frac{2}{3}q_x & m_{xyy} & \hat{R}_{xy} & -\theta\frac{\sigma}{\rho} & 0 & -\theta\frac{\sigma_{yy}}{\rho} & 0 & 0 & 0 & \frac{2}{15}\theta\frac{(3\sigma_{yy}-5\sigma_{xx})}{\rho} & 0 \end{array}\right) \tag{91}$$

A.2 Transformed System

The transformed system results after eliminating m_{xyy} and $\hat{R}_{yy}$ and keeping the full null-space as described in Sec. 5.2. The reduced set of variables is given by

$$\mathbf{U} = \{v_x, \sigma, q_x, R_{xy}, \theta, q_y, \sigma_{yy}, m_{yyy}, \rho, \sigma_{xx}, m_{xxy}\} \tag{92}$$

and the system has the form

$$\left(\begin{array}{c} -\frac{\mu}{p}F \\ \sigma + \frac{64\omega}{225\theta}\frac{\mu}{p}F\,q_y \\ \frac{2}{3}q_x \\ \hat{R}_{xy} - \frac{12}{7}\frac{(\sigma_{xx}+\sigma_{yy})\sigma}{\rho} - \frac{32}{25}\frac{q_x q_y}{p} \\ 0 \\ \frac{2}{3}q_y \\ \sigma_{yy} \\ m_{yyy} - \frac{8}{25}\frac{\sigma_{yy}\,q_y - \sigma\,q_x}{p} \\ 0 \\ \sigma_{xx} \\ m_{xxy} + \frac{16\sigma_{yy}q_y - 40\,\sigma_{xx}q_y - 96\sigma q_x}{225p} \end{array}\right) = -\frac{p}{\mu}$$

$$\left(\begin{array}{c} \partial_y v_x \\ \partial_y \sigma \\ \partial_y q_x \\ \partial_y \hat{R}_{xy} \\ \partial_y \theta \\ \partial_y q_y \\ \partial_y \sigma_{yy} \\ \partial_y m_{yyy} \\ \partial_y \rho \\ \partial_y \sigma_{xx} \\ \partial_y m_{xxy} \end{array}\right)$$

$$\left(\begin{array}{cccccccccc} 0 & \frac{1}{\rho} & 0 & 0 & 0 & 0 & 0 & 0 & 0 & 0 \\ p+\sigma_{yy} & \frac{32}{45}\frac{q_y}{p} & \frac{2}{5} & 0 & 0 & 0 & 0 & 0 & 0 & 0 \\ \frac{7}{5}q_y + m_{xxy} & \theta - \frac{\sigma_{xx}}{\rho} & 0 & \frac{1}{2} & 0 & 0 & 0 & 0 & 0 & 1 \\ 0 & 0 & \frac{12}{5}\theta & 0 & 0 & 0 & 0 & 0 & \theta & 0 \\ \hline \sigma & 0 & 0 & 0 & 0 & 0 & 0 & 0 & 0 & 0 \\ \frac{2}{5}q_x + m_{xyy} & -\frac{107\sigma}{35\rho} & 0 & 0 & \frac{5p}{2} + \frac{7\sigma_{yy}}{2} - \frac{4\sigma^2}{5p} & \frac{136q_y}{25p} & \theta & 0 & 0 & 0 \\ 0 & 0 & 0 & 0 & 0 & \frac{6}{5} & 0 & 1 & 0 & 0 \\ 0 & 0 & 0 & 0 & 0 & 0 & \frac{6}{5}\theta & 0 & 0 & 0 \\ \hline 0 & 0 & 0 & 0 & \rho & 0 & 1 & 0 & \theta & 0 \\ 2\sigma & 0 & 0 & 0 & 0 & \frac{2}{5} & 0 & 0 & 0 & 1 \\ 0 & 0 & 0 & 0 & 0 & 0 & -\frac{4}{15}\theta & 0 & 0 & \frac{2}{3}\theta \end{array}\right) \tag{93}$$

B Numerical Matrices

For use in the numerical method of Sec. 6 the right hand side of the system (93) is written in the form

$$\mathbf{P}\left(\mathbf{U}\right) = -\widetilde{\mathbf{P}}\left(\mathbf{U}\right)\mathbf{U} + \mathbf{P}_{\text{inh}} \tag{94}$$

with the matrix

$$\widetilde{\mathbf{P}}\left(\mathbf{U}\right) = \frac{p}{\mu}\left(\begin{array}{cccc|cccc|cc} 0 & 0 & 0 & 0 & 0 & 0 & 0 & 0 & 0 & 0 \\ 0 & 1 & 0 & 0 & 0 & 0 & 0 & 0 & 0 & 0 \\ 0 & 0 & \frac{2}{3} & 0 & 0 & 0 & 0 & 0 & 0 & 0 \\ 0 & -\frac{6}{7}\frac{\sigma_{xx}+\sigma_{yy}}{\rho} & -\frac{16}{25}\frac{q_y}{p} & 1 & 0 & -\frac{16}{25}\frac{q_x}{p} & -\frac{6}{7}\frac{\sigma}{\rho} & 0 & -\frac{6}{7}\frac{\sigma}{\rho} & 0 \\ \hline 0 & 0 & 0 & 0 & 0 & 0 & 0 & 0 & 0 & 0 \\ 0 & 0 & 0 & 0 & 0 & \frac{2}{3} & 0 & 0 & 0 & 0 \\ 0 & 0 & 0 & 0 & 0 & 0 & 1 & 0 & 0 & 0 \\ 0 & \frac{4}{25}\frac{q_x}{p} & \frac{4}{25}\frac{\sigma}{p} & 0 & 0 & -\frac{4}{25}\frac{\sigma_{yy}}{p} & -\frac{4}{25}\frac{q_y}{p} & 1 & 0 & 0 \\ \hline 0 & 0 & 0 & 0 & 0 & 0 & 0 & 0 & 1 & 0 \\ 0 & -\frac{48}{225}\frac{q_x}{p} & -\frac{48}{225}\frac{\sigma}{p} & 0 & 0 & \frac{8\sigma_{yy}-20\,\sigma_{xx}}{225p} & \frac{8}{225}\frac{q_y}{p} & 0 & -\frac{4}{45}\frac{q_y}{p} & 1 \end{array}\right) \tag{95}$$

and the vector

$$\mathbf{P}_{\text{inh}} = \left(F, -\frac{64\omega}{225\theta}F\,q_y,\ \mathbf{0}\in\mathbb{R}^8\right). \tag{96}$$

Note, that the density has been dropped from the variable vector which now reads $\mathbf{U} = \{v_x,\, \sigma,\, q_x,\, R_{xy},\, \theta,\, q_y,\, \sigma_{yy},\, m_{yyy},\, \sigma_{xx},\, m_{xxy}\}$. Also for incorporation into the numerical method the boundary conditions (33)-(37) are cast into

$$\mathbf{U} = \mathbf{B}(\mathbf{U})\mathbf{U} + \mathbf{B}_{\text{inh,p}}(\mathbf{U}) \tag{97}$$

with the matrix

$$\mathbf{B}\left(\mathbf{U}\right) = \left(\begin{array}{cccc|cccc|cc} 1 & 0 & 0 & 0 & 0 & 0 & 0 & 0 & 0 & 0 \\ -\beta_1 P & 0 & -\frac{1}{5}\beta_1 & 0 & 0 & 0 & 0 & 0 & 0 & 0 \\ 0 & 0 & 1 & 0 & 0 & 0 & 0 & 0 & 0 & 0 \\ \beta_2\theta P & 0 & -\frac{11}{5}\beta_2\theta & 0 & 0 & 0 & 0 & 0 & 0 & 0 \\ \hline 0 & 0 & 0 & 0 & 1 & 0 & 0 & 0 & 0 & 0 \\ 0 & 0 & 0 & 0 & -2\beta_3 P & 0 & -\frac{1}{2}\beta_3\theta & 0 & 0 & 0 \\ 0 & 0 & 0 & 0 & 0 & 0 & 1 & 0 & 0 & 0 \\ 0 & 0 & 0 & 0 & \frac{2}{5}\beta_4 P & 0 & -\frac{7}{5}\beta_4\theta & 0 & 0 & 0 \\ \hline 0 & 0 & 0 & 0 & 0 & 0 & 0 & 0 & 1 & 0 \\ 0 & 0 & 0 & 0 & 0 & 0 & 0 & 0 & -\beta_5\theta & 0 \end{array}\right) \tag{98}$$

and the vector

$$\begin{aligned}\mathbf{B}_{\text{inh,p}}\left(\mathbf{U}\right) = \Big(\ & 0, \quad \beta_1(P\,v_W^{(p)} + \tfrac{1}{2}m_{xyy}), \quad 0, \quad -\beta_2(\theta\,P\,v_W^{(p)} + P\,V(V^2 - 6\Delta\theta) + \tfrac{1}{2}\theta\,m_{xyy}), \\ & 0, \quad \beta_3(2P\,\theta_W^{(p)} + \tfrac{1}{2}P\,V^2 - \tfrac{5}{28}\hat{R}_{yy}), \quad 0, \quad -\beta_4(\tfrac{2}{5}P\,\theta_W^{(p)} + \tfrac{3}{5}P\,V^2 + \tfrac{1}{14}\hat{R}_{yy}), \quad 0, \quad \beta_5 P\,V^2 \ \Big)^T\end{aligned} \tag{99}$$

where $p \in \{0,1\}$ represents the superscript for the left and right wall. The vector $\mathbf{B}_{\mathrm{inh,p}}$ contains the slip velocity $V^{(0,1)} = v_y - v_W^{(0,1)}$ and the temperature jump $\Delta\theta^{(0,1)} = \theta - \theta_W^{(0,1)}$. The accommodation coefficient is hidden in the parameter

$$\beta_i = \sqrt{\frac{2}{\pi\theta}} \frac{\chi_i}{2-\chi_i} \tag{100}$$

where we assumed different accommodation coefficients for all boundary conditions in (33)-(37). In the original boundary conditions the trace of the fourth moment R was present. It does not appear as variable in our system, but, instead, would have to be computed from (4). Due to relatively small numerical coefficients we dropped it in (97) for simplicity.

C Distribution Function

The velocity distribution function for the R13 equations is based on the 26-moment-case of Grad, see e.g., [26]. In peculiar velocities $\mathbf{C} = \mathbf{c} - \mathbf{v}$ the distribution function reads

$$f_{\mathrm{R13}}(\mathbf{C}) = \left(1 + \varphi_{13}(\mathbf{C}) + \varphi_{R1}(\mathbf{C}) + \varphi_{R2}(\mathbf{C})\right) f_M(\mathbf{C}) \tag{101}$$

with the Maxwell distribution

$$f_M(\mathbf{C}) = \frac{\rho/m}{\sqrt{2\pi\theta}^3} \exp\left(-\frac{\mathbf{C}^2}{2\theta}\right) \tag{102}$$

and correction terms

$$\varphi_{13}(\mathbf{C}) = \frac{1}{\theta^2 p}\left(\left(q_x C_x + q_y C_y\right)\left(\tfrac{C^2}{5} - \theta\right) + \tfrac{\theta}{2}\left(\sigma_{xx}C_x^2 + \sigma_{yy}C_y^2 + \sigma_{zz}C_z^2 + 2\sigma C_x C_y\right)\right) \tag{103}$$

$$\varphi_{R1}(\mathbf{C}) = \frac{1}{2\theta^2 p}\left(\tfrac{1}{3}m_{xxx}C_x^3 + \tfrac{1}{3}m_{yyy}C_y^3 + m_{xxy}C_x^2 C_y + m_{xyy}C_x C_y^2 + m_{xzz}C_x C_z^2 + m_{yzz}C_y C_z^2\right) \tag{104}$$

$$\varphi_{R2}(\mathbf{C}) = \frac{1}{4\theta^3 p}\left(\left(R_{xx}C_x^2 + R_{yy}C_y^2 + R_{zz}C_z^2 + 2R_{xy}C_x C_y\right)\left(\tfrac{C^2}{7} - \theta\right) + \tfrac{R}{30}\left(C^4 - 10\theta C^2 + 15\theta^2\right)\right) \tag{105}$$

The case $\varphi_{R1} = \varphi_{R2} = 0$ corresponds to Grad's 13-moment distribution. In case of R13 the additional terms involving m_{ijk} and R_{ij} are to be evaluated with the constitutive equations (21)-(25).

References

[1] S. Ansumali, I. V. Karlin, S. Arcidiacono, A. Abbas, and N. I. Prasianakis, *Hydrodynamics beyond Navier-Stokes: Exact solutions to the lattice Boltzmann hierarchy*, Phys. Rev. Letters **98**, (2007), 124502

[2] R. K. Agarwal, K. Y. Yun, and R. Balakrishnan, *Beyond Navier-Stokes: Burnett equations for flows in the continuum-transition regime*, Phys. Fluids **13**, (2001), p.3061-3085, Erratum: Phys. Fluids **14**, (2002), p.1818

[3] J. D. Au, M. Torrilhon, and W. Weiss, *The Shock Tube Study in Extended Thermodynamics*, Phys. Fluids **13**(8) , (2001) p.2423-2432

[4] G. A. Bird, *Molecular Gas Dynamics and the Direct Simulation of Gas Flows* (2nd edn), Oxford University Press, New York (1998)

[5] A.V. Bobylev, *The Chapman-Enskog and Grad methods for solving the Boltzmann equation*, Sov. Phys. Dokl. **27**, (1982) p.29-31

[6] A. V. Bobylev, *Instabilities in the Chapman-Enskog Expansion and Hyperbolic Burnett Equations*, J. Stat. Phys. **124** (2-4), (2006), p.371-399

[7] C. Cercignani, *The Boltzmann Equation and its Applications*, Applied Mathematical Sciences 67, Springer, New York, (1988)

[8] S. Chapman and T. G. Cowling, *The Mathematical Theory of Non-Uniform Gases*, Cambridge University Press, Cambridge (1970)

[9] B.-C. Eu, *A Modified Moment Method and Irreversible Thermodynamics*, J. Chemical Phys. **73**(6), (1980) p.2958-2969

[10] H. Grad, *On the Kinetic Theory of Rarefied Gases*, Comm. Pure Appl. Math. **2**, (1949), p.331-407

[11] H. Grad, *Principles of the Kinetic Theory of Gases*, in Handbuch der Physik, editor S. Flügge, Springer, Berlin (1958), vol. 12

[12] X. Gu and D. Emerson, *A Computational Strategy for the Regularized 13 Moment Equations with Enhanced Wall-Boundary Conditions*, J. Comput. Phys. (2007), in press

[13] S. Jin and M. Slemrod, *Regularization of the Burnett equations via relaxation*, J. Stat. Phys. **103** (5-6), (2001) p.1009-1033

[14] G. E. Karniadakis and A. Beskok, *Micro Flows: Fundamentals and Simulation*, Springer, New York (2001)

[15] M. Knudsen, *Die Gesetze der Molekularströmung und der inneren Reibungsströmung der Gase durch Röhren*, Ann. Phys. **333**, (1909), p.75-130

[16] C. D. Levermore, *Moment closure hierarchies for kinetic theories*, J. Stat. Phys. **83**(5-6), (1996) p.1021-1065

[17] D. A. Lockerby and J. M. Reese, *High-resolution Burnett simulations of micro Couette flow and heat transfer*, J. Comput. Phys. **188**(2), (2003), p.333-347

[18] J. C. Maxwell, *On Stresses in Rarefied Gases Arising From Inequalities of Temperature*, Phil. Trans. Roy. Soc. (London) **170**, (1879), p.231-256

[19] I. Müller and T. Ruggeri, *Rational Extended Thermodynamics* (2nd edn), Springer Tracts in Natural Philosophy (vol.37), Springer, New York (1998)

[20] I. Müller, D. Reitebuch, and W. Weiss, *Extended Thermodynamics - Consistent in Order of Magnitude*, Cont. Mech. Thermodyn. **15**(2), (2003) p.411-425

[21] R.-S. Myong, *A computational method for Eu's generalized hydrodynamic equations of rarefied and microscale gas dynamics*, J. Comput. Phys. **168**(1), (2001) p.47-72

[22] T. Ohwada, Y. Sone and K. Aoki, *Numerical analysis of the Poiseuille and thermal transpiration flows between two parallel plates on the basis of the Boltzmann equation for hard-sphere molecules*, Phys. Fluids A **1**(12), (1989), p.2042-2049

[23] P. Rosenau, *Extending hydrodynamics via the regularization of the Chapman-Enskog expansion*, Phys. Rev. A **40**, (1989), p.7193-7196

[24] S. Seeger and H. Hoffmann: *The Comulant Method in Computational Kinetic Theory*, Cont. Mech. Therm. **12**/6 (2000) p.403

[25] F. Sharipov and V. Seleznev, Data on Internal Rarefied Gas Flows, J. Phys. Chem. Ref. Data **27**(3), (1998), p.657-706

[26] H. Struchtrup, *Macroscopic Transport Equations for Rarefied Gas Flows*, Interaction of Mechanics and Mathematics, Springer, New York (2005)

[27] H. Struchtrup, *Grad's Moment Equations for Microscale Flows*, 23rd Intl. Symposium on Rarefied Gas Dynamics, AIP Proceedings 663, (2003), p.792-799

[28] H. Struchtrup, *Stable transport equations for rarefied gases at high orders in the Knudsen number*, Phys. Fluids **16**(11), (2004) p.3921-3934

[29] H. Struchtrup, *Derivation of 13 moment equations for rarefied gas flow to second order accuracy for arbitrary interaction potentials*, Multiscale Model. Simul. **3**(1), (2005) p.221-243

[30] H. Struchtup and T. Thatcher, *Bulk equations and Knudsen layers for the regularized 13 moment equations*, Cont. Mech. Thermodyn. (2007), in press

[31] H. Struchtrup and M. Torrilhon, *Regularization of Grad's 13-Moment-Equations: Derivation and Linear Analysis*, Phys. Fluids **15**/9, (2003), pp.2668-2680

[32] H. Struchtrup and M. Torrilhon, *H-theorem, regularization, and boundary conditions for linearized 13 moment equations*, Phys. Rev. Letters, (2007) in press

[33] Y. Suzuki and B. van Leer, *Application of the 10-moment model to MEMS flows*, 43rd AIAA Aerospace Sciences Meeting and Exhibit, AIAA Paper 2005-1398, (2005)

[34] T. Thatcher, *Microscale gas flow: a comparison of Grad's 13 moment equations and other continuum approaches*, Masters Thesis, Dept. Mech. Eng., Univ. of Victoria, Canada, (2005)

[35] M. Torrilhon, *Two-Dimensional Bulk Microflow Simulations Based on Regularized 13-Moment-Equations*, SIAM Multiscale Model. Simul. **5**(3), 695-728 (2006)

[36] M. Torrilhon, *Regularized 13-Moment-Equations*, 25th Intl. Symposium on Rarefied Gas Dynamics, St. Petersburg, Russia, (2006)

[37] M. Torrilhon and H. Struchtrup, *Regularized 13-Moment-Equations: Shock Structure Calculations and Comparison to Burnett Models*, J. Fluid Mech. **513**, (2004), pp.171-198

[38] W. G. Vincenti and C. H. Kruger, Jr., *Introduction to Physical Gas Dynamics*, Wiley, New York (1965)

[39] K. Xu and Z.-H. Li, *Microchannel flow in the slip regime: gas-kinetic BGK-Burnett solutions*, J. Fluid Mech. 513, (2004) p.87-110

[40] Y. Zheng, A. L. Garcia, and J. B. Alder, *Comparison of kinetic theory and hydrodynamics for Poiseuille flow*, J. Stat. Phys. **109**, (2002), p.495-505